Presynaptic Rac1 controls synaptic strength through the regulation of synaptic vesicle priming

(Abbreviated title): Presynaptic Rac1 regulates synaptic strength

Christian Keine[1,2,3], Mohammed Al-Yaari[1], Tamara Radulovic[1,2,3], Connon I. Thomas[4], Paula V. Ramos[1], Debbie Guerrero-Given[4], Naomi Kamasawa[4], and Samuel M. Young, Jr.[1,5^].

[1]Department of Anatomy and Cell Biology, University of Iowa, Iowa City, IA, USA
[2]Department of Human Medicine, Carl-von-Ossietzky University Oldenburg, Oldenburg, Germany
[3]Research Center Neurosensory Science, Oldenburg, Germany
[4]Electron Microscopy Core Facility, Max Planck Florida Institute, Jupiter, FL, USA
[5]Department of Otolaryngology, Iowa Neuroscience Institute, University of Iowa, Iowa City, IA, USA.

^Correspondence
Samuel M. Young, Jr. PhD
Department of Anatomy and Cell Biology
University of Iowa
PBDB 5322
169 Newton Road
Iowa City, IA 52242
Email: samuel-m-young@uiowa.edu

Abstract

Synapses contain a limited number of synaptic vesicles (SVs) that can be released in response to action potentials (APs). Therefore, sustaining synaptic transmission over a wide range of AP firing rates and timescales depends on both SV release and replenishment. Although actin dynamics impact synaptic transmission, how regulators of actin dynamics control SV release and replenishment remain unresolved. Rac1 is a regulator of actin signaling cascades that control synaptogenesis, neuronal development, and postsynaptic function, however, its presynaptic role in regulating synaptic transmission is unclear. To unravel the regulatory roles of presynaptic Rac1 in synaptic transmission, we ablated presynaptic Rac1 at the mature mouse calyx of Held. Presynaptic Rac1 deletion leads to increased synaptic strength due to increased SV release probability which results in faster SV replenishment and increased spontaneous SV release rates. Based on our data, we conclude that presynaptic Rac1 controls synaptic strength by regulating the intrinsic SV release probability through SV priming. Therefore, we propose that presynaptic Rac1 controls actin dynamics and acts as a key regulator of synaptic transmission and plasticity

.

41 **Introduction**

42 Information encoding in the nervous system requires synaptic transmission to drive and sustain
43 action potentials (APs) over rapid and large fluctuations of AP firing rates (Reinagel and Laughlin,
44 2001; Theunissen and Elie, 2014; Brette, 2015; Azarfar et al., 2018). However, the number of
45 synaptic vesicles (SVs) that can be released in response to an AP, the readily releasable pool
46 (RRP), is limited (Alabi and Tsien, 2012). Therefore, tight regulation of SV release and
47 replenishment is required for synaptic reliability and temporal precision needed to encode
48 information (Neher, 2010; Hallermann and Silver, 2013). Priming is the process that creates
49 fusion-competent SVs and is a key step in the SV life cycle that regulates RRP size,
50 replenishment, and the SV release probability (P_r) (Klug et al., 2012; Neher and Brose, 2018).
51 Furthermore, modulation of the temporal dynamics of priming is highly dependent on presynaptic
52 Ca^{2+} levels. Importantly, human mutations in molecules that regulate priming are associated with
53 neurological disorders (Waites and Garner, 2011; Wondolowski and Dickman, 2013; Torres et al.,
54 2017; Bonnycastle et al., 2021). Therefore, elucidating the molecular mechanisms that regulate
55 priming is critical to understanding the diversity of information encoding in the nervous system.

56 Actin is a central component of both the presynaptic and postsynaptic compartment with diverse
57 roles in regulating synaptic function and neuronal circuit development. Manipulation of actin
58 dynamics or the presynaptic AZ proteins that regulate actin dynamics affects SV release and
59 replenishment rates, as well as P_r (Morales et al., 2000; Sakaba and Neher, 2003; Cingolani and
60 Goda, 2008; Waites et al., 2011; Lee et al., 2012, 2013; Montesinos et al., 2015; Rust and
61 Maritzen, 2015, 2015). However, due to disparate results, the presynaptic role of actin in regulating
62 SV release and replenishment is controversial. Additionally, in contrast to the postsynaptic
63 compartment, our understanding of presynaptic actin signaling cascades that regulate SV release
64 and replenishment are in the early stages.

65 Rac1, a small GTPase in the Rho family, is a critical regulator of actin signaling cascades (Bosco
66 et al., 2009; Yasuda, 2017), and human mutations in Rac1 are associated with neurological

67 disorders (Bai et al., 2015; Reijnders et al., 2017; Zamboni et al., 2018). Rac1 is involved in
68 multiple processes which control synaptogenesis, axon guidance, neuronal development, and
69 postsynaptic function to regulate neuronal circuit function (Bai et al., 2015). Although Rac1 is
70 expressed in both the pre and postsynaptic compartment (Threadgill et al., 1997; Doussau et al.,
71 2000; Kumanogoh et al., 2001; O'neil et al., 2021), its presynaptic role in regulating synaptic
72 transmission is not well understood. However, recent work using primary cultured hippocampal
73 neurons proposed that presynaptic Rac1 is a negative regulator of SV replenishment (O'neil et al.,
74 2021), though at which steps in the SV lifecycle it exerts its regulatory role is unknown. Finally,
75 how Rac1 regulates the temporal dynamics of RRP release and replenishment in a native
76 neuronal circuit remains elusive.

77 To unravel the regulatory roles of presynaptic Rac1 in regulating synaptic transmission, we utilized
78 the calyx of Held, an axosomatic presynaptic terminal in the auditory brainstem, which is the sole
79 input to drive AP spiking in the principal cells of the medial nucleus of the trapezoid body (MNTB)
80 (Borst and Soria Van Hoeve, 2012; Joris and Trussell, 2018). In the calyx of Held, RRP dynamics
81 are tightly regulated to support the early stages of auditory processing, but the properties of SV
82 release and replenishment are similar to conventional presynaptic terminals in the central nervous
83 system (Iwasaki and Takahashi, 1998; Iwasaki et al., 2000; Iwasaki and Takahashi, 2001; Sätzler
84 et al., 2002; Taschenberger et al., 2002; Rollenhagen and Lübke, 2006; Neher and Sakaba, 2008;
85 Alabi and Tsien, 2012; Eggermann et al., 2012; Hallermann and Silver, 2013; Kaeser and Regehr,
86 2014; Schneggenburger and Rosenmund, 2015). In addition, molecular manipulations specific to
87 the calyx of Held can be carried out at different neuronal circuit developmental stages (Wimmer
88 et al., 2006; Young and Neher, 2009; Chen et al., 2013; Lübbert et al., 2019). To elucidate the
89 roles of presynaptic Rac1 in regulating synaptic transmission while avoiding its role in
90 synaptogenesis, axon guidance, and neuronal development, we ablated Rac1 expression 2 days
91 after hearing onset, postnatal day (P) 14 in the mouse, when the calyx of Held is functionally
92 mature where neuronal circuit properties are "adult-like" (Sonntag et al., 2009; Crins et al., 2011;

93 Sonntag et al., 2011) and determined how the loss of Rac1 impacted calyx of Held/MTNB
94 transmission at the adult stage (P28 onwards). We found that presynaptic *Rac1* deletion does not
95 affect the calyx of Held morphology or active zone (AZ) ultrastructure but leads to increased
96 synaptic strength. This increase in synaptic strength is due to increased SV release probability
97 which results in faster SV replenishment and increased spontaneous SV release rates.
98 Additionally, we found that loss of Rac1 leads to temporal delay of EPSC onset with an increase
99 in asynchronous release during high-frequency train stimuli. Taken together, our data demonstrate
100 that presynaptic Rac1 is a key molecule that controls synaptic strength through SV priming steps
101 that regulate SV release probability.

102 **Results**

103 **Presynaptic deletion of Rac1 after hearing onset does not impact calyx of Held morphology**
104 **or AZ ultrastructure**

105 Rac1 is found in the presynaptic terminal (Doussau et al., 2000; O'neil et al., 2021) and
106 regulates synaptogenesis, axon guidance, and neuronal development (Xu and Chen, 2019; Zhang
107 et al., 2021). In this study, we aimed to elucidate Rac1's presynaptic function in controlling synaptic
108 transmission and plasticity independent of its role in regulating synapse development and
109 maturation at the calyx of Held/MNTB synapse. To do so, we injected HdAd co-expressing Cre
110 recombinase and EGFP into the cochlear nucleus (CN) of P14 *Rac1*$^{flox/flox}$ animals when the calyx
111 of Held/MNTB synapse is considered "adult-like" and analyzed the calyx of Held/MNTB synapse
112 at P28 onwards (Fig. 1A, Sonntag et al., 2009, 2011; Crins et al., 2011). Since Rac1 acts as a
113 central molecule controlling synapse development and morphology, it was important to determine
114 whether the loss of Rac1 after hearing onset altered the calyx of Held morphology or AZ
115 ultrastructure. Morphology was analyzed from 3D reconstructions of calyx terminals from confocal
116 z-stack images acquired from *Rac1*$^{+/+}$ and *Rac1*$^{-/-}$ animals at P28 and we found no change in calyx
117 surface area or volume (Fig. 1B). To determine if the loss of Rac1 impacted AZ ultrastructure, we
118 performed ultrathin section TEM and analyzed AZ length, SV distribution, and the number of
119 docked SVs and found no difference between *Rac1*$^{+/+}$ and *Rac1*$^{-/-}$ (Fig. 1C). Therefore, we
120 conclude that after hearing onset Rac1 is not essential for regulating calyx of Held morphology
121 and AZ ultrastructure.

122 **Loss of Rac1 increases synaptic strength through an increase in SV release probability.**

123 Perturbations of the presynaptic actin cytoskeleton impact synaptic transmission and
124 plasticity in multiple model systems and synapses (Cole et al., 2000; Sakaba and Neher, 2003;
125 Bleckert et al., 2012; Rust and Maritzen, 2015; Miki et al., 2016; Gentile et al., 2022; Wu and Chan,
126 2022). Since Rac1 is an actin cytoskeleton regulator, we examined how the loss of Rac1 impacted
127 AP-evoked synaptic transmission and short-term plasticity. Afferent fiber stimulation of calyx

128 axons was performed using 50 AP at two stimulation frequencies (50 Hz and 500 Hz) representing
129 typical *in vivo* firing rates at the calyx at low or high activity, respectively. AMPAR-mediated ESPCs
130 from MNTB principal cells innervated by transduced (*Rac1*$^{-/-}$) and non-transduced calyces
131 (*Rac1*$^{+/+}$) were recorded in 1.2 mM external Ca^{2+} concentration and 36-37°C to mimic *in vivo*
132 conditions (Fig. 2A, B). Analyzing the first EPSC ($EPSC_1$) of the stimulus train, we found a dramatic
133 increase in EPSC amplitude upon *Rac1* deletion (*Rac*$^{+/+}$ = 1.3 ± 0.4 nA vs. *Rac1*$^{-/-}$ = 3 ± 1.1 nA,
134 p=2.5e-5, n=15/15, Fig. 2C) with no change in EPSC waveform. Plotting EPSC amplitudes vs.
135 stimulation number revealed differences in short-term plasticity between *Rac1*$^{+/+}$ and *Rac1*$^{-/-}$. At
136 50 Hz stimulation, both *Rac1*$^{+/+}$ and *Rac1*$^{-/-}$ showed short-term depression which was emphasized
137 in *Rac1*$^{-/-}$ with increased steady-state depression relative to $EPSC_1$. Despite the stronger relative
138 short-term depression, absolute steady-state EPSC amplitudes were almost two-fold larger in
139 *Rac1*$^{-/-}$ (*Rac1*$^{+/+}$ = 0.47 ± 0.14 nA vs. *Rac1*$^{-/-}$ = 0.84 ± 0.22 nA, p = 4e-5, n = 15/15) and
140 replenishment rates were increased (*Rac1*$^{+/+}$ = 23 ± 7 nAs^{-1} vs. *Rac1*$^{-/-}$ = 42 ± 11 nAs^{-1}, p = 2.4e-
141 5, n = 15/15). At 500 Hz stimulation, *Rac1*$^{+/+}$ showed robust short-term facilitation which was
142 absent in *Rac1*$^{-/}$ (PPR: Rac1$^{+/+}$ = 1.2 ± 0.1 vs. Rac1$^{-/-}$ = 1 ± 0.1, p = 3.4e-6, n = 15/15). Similar to
143 50 Hz stimulation, *Rac1*$^{-/-}$ showed increased levels of relative steady-state depression at 500 Hz
144 stimulation. Notably, absolute steady-state EPSC amplitude and replenishment rates at 500 Hz
145 stimulation frequency were not different between *Rac1*$^{+/+}$ and *Rac1*$^{-/-}$.

146 Since the loss of Rac1 increased synaptic strength and altered short-term plasticity it was
147 important to determine if these changes were caused by an increase in RRP size, SV release
148 probability (P_r), or both. We estimated the RRP size using 500 Hz stimulation frequency since it
149 effectively depletes the RRP for both *Rac1*$^{+/+}$ and *Rac1*$^{-/-}$ and employed three methods to estimate
150 the RRP: EQ, NpRf, and SMN with correction (Elmqvist and Quastel, 1965; Neher, 2015;
151 Thanawala and Regehr, 2016). Both, the EQ and NpRf method reported no change in RRP size,
152 while the SMN method detected a slight RRP increase in *Rac1*$^{-/-}$ calyces. Subsequently, we
153 calculated the initial P_r by dividing the amplitude of the 1st EPSC by the estimated RRP sizes and

154 all three methods revealed a two-fold increase in P_r (SMN: *Rac1*$^{+/+}$ = 0.09 ± 0.02 vs. *Rac1*$^{-}$
155 $^{/-}$ = 0.15 ± 0.03, p = 4.8e-7; NpRf: *Rac1*$^{+/+}$ = 0.09 ± 0.02 vs. *Rac1*$^{-/-}$ = 0.17 ± 0.03, p = 2.5e-7; EQ:
156 *Rac1*$^{+/+}$ = 0.08 ± 0.02 vs. *Rac1*$^{-/-}$ = 0.16 ± 0.03, p = 2.4e-7, n = 15/15). Next, we calculated the
157 steady-state P_r (steady-state EPSC divided by the calculated remaining RRP) and found an
158 increase in *Rac1*$^{-/-}$ calyces at both 50 Hz (*Rac1*$^{+/+}$ = 0.09 ± 0.02 vs. *Rac1*$^{-/-}$ = 0.16 ± 0.03, p = 9.4e-
159 7, n=15/15) and 500 Hz stimulation (*Rac1*$^{+/+}$ = 0.09 ± 0.02 vs. *Rac1*$^{-/-}$ = 0.15 ± 0.03, p = 3.2e-7,
160 n = 15/15). These findings show that presynaptic Rac1 deletion increases short-term depression
161 by elevating both initial and steady-state P_r with little or no effect on RRP size. Therefore, we
162 conclude that Rac1 controls synaptic strength as a negative regulator of P_r.

163 **Loss of Rac1 increases mEPSC frequency but not amplitude**

164 The two steps in the SV life cycle that impact RRP size and P_r are molecular priming and
165 positional priming (Neher and Brose, 2018). Molecular priming encompasses the steps that render
166 an SV fusion competent and regulates the intrinsic SV fusogenicity, defined as the fusion
167 willingness of an SV (Basu et al., 2007; Xue et al., 2010; Schotten et al., 2015). Positional priming
168 consists of the steps that place molecularly primed SVs close to the voltage-gated calcium
169 channels (VGCCs) (Neher, 2010). The distance between SV and VGCCs, coupling, is a critical
170 determinant of the speed and efficacy of AP-evoked release (Eggermann et al., 2012).
171 Spontaneous SV release is independent of VGCCs (Schneggenburger and Rosenmund, 2015;
172 Kavalali, 2020) and the frequency of miniature EPSC (mEPSCs) can be used as a readout of
173 changes in SV fusogenicity with increased SV fusogenicity causing higher mEPSC frequencies
174 (Basu et al., 2007; Schotten et al., 2015; Dong et al., 2018). Therefore, to ascertain if the increase
175 in P_r was caused by an increase in intrinsic SV fusogenicity, we recorded mEPSCs from *Rac1*$^{+/+}$
176 and *Rac1*$^{-/-}$ calyces (Fig. 3) and found a four-fold increase in mEPSC frequency
177 (*Rac1*$^{+/+}$ = 3.4 ± 4.4 Hz vs. *Rac1*$^{-/-}$ = 14.3 ± 6.5 Hz, p = 3.4e-4, n = 15/11) with no change in
178 mEPSC amplitude or waveform. To rule out that the increased mEPSC frequencies were due to
179 changes in Cav2.1 currents we recorded mEPSCs in the presence of 200 μM Cd^{2+}, a non-specific

180 VGCC blocker. Since the addition of Cd^{2+} did not affect mEPSC frequencies (control = 14.6 ± 3.2
181 Hz vs. cadmium = 14.9 ± 2 Hz, p = 0.84, n = 3/3), we conclude that Rac1 regulates P_r by
182 controlling intrinsic SV fusogenicity independent of Ca^{2+}.

183 **Loss of Rac1 increases temporal delays in AP evoked release**

184 Although we found an increase in SV fusogenicity, this does not rule out an additional role
185 for Rac1 in regulating positional priming. In the mature calyx of Held, nanodomain release results
186 in a fast onset of synchronous AP-evoked EPSCs to encode auditory information (Fedchyshyn
187 and Wang, 2005). The time between presynaptic AP and EPSC onset (EPSC onset delay) is
188 determined by the distance between SVs and VGCC which defines the time it takes for Ca^{2+} to
189 bind to the Ca^{2+} sensor and trigger SV release (Fedchyshyn and Wang, 2007). Thus, EPSC onset
190 delays can serve as a readout of changes in positional priming, as increases in onset delay would
191 indicate more loosely coupled SVs and vice versa. Therefore, we measured EPSC onset delays
192 during 50 Hz and 500 Hz stimulation (Fig. 4A, B) and found them to become progressively larger
193 during stimulation for both *Rac1*$^{+/+}$ and *Rac1*$^{-/-}$ calyces. At 50 Hz, the increase in EPSC onset delay
194 was comparable between *Rac1*$^{+/+}$ and *Rac1*$^{-/-}$ amounting to about 60 µs between the first and the
195 last ten EPSCs. At 500 Hz stimulation, however, EPSC onset delays increased more rapidly in
196 *Rac1*$^{-/-}$ with steady-state EPSC onsets delays being significantly larger for *Rac1*$^{-/-}$ compared to
197 *Rac1*$^{+/+}$ (*Rac1*$^{+/+}$ = 94± 32 µs vs. *Rac1*$^{-/-}$= 131 ± 29 µs, p = 0.004, n = 15/15).

198 In addition to EPSC onset delays, the synchronicity of AP-evoked release can be used as
199 an indirect readout of positional priming since synchronous release represents SVs that are tightly
200 coupled and asynchronous release is representative of loosely coupled SVs (Sakaba, 2006;
201 Schneggenburger and Rosenmund, 2015). Furthermore, EPSC synchronicity is independent of
202 conduction delay, the delay between stimulus and the time when the AP reaches the presynaptic
203 terminal. Therefore, we determined EPSC synchronicity by dividing the EPSC amplitude by the
204 EPSC charge for both 50 Hz and 500 Hz stimulation (Fig. 4C). The synchronicity of the first EPSC
205 was comparable between *Rac1*$^{+/+}$ and *Rac1*$^{-/-}$ while steady-state EPSC synchronicity at 50 Hz

206 was slightly lower in *Rac1*$^{-/-}$ (*Rac1*$^{+/+}$ = 3.2 ± 0.3 nA pC^{-1} vs. Rac1 KO = 2.9 ± 0.2 nA pC^{-1},
207 p = 0.006). At 500 Hz stimulation, steady-state EPSC synchronicity in *Rac1*$^{-/-}$ calyces was further
208 deteriorated and 20% lower compared to *Rac1*$^{+/+}$ (*Rac1*$^{+/+}$ = 2.4 ± 0.3 nA pC^{-1} vs. *Rac1*$^{-/-}$
209 = 1.9 ± 0.3 nA pC^{-1}, p = 2.3e-4). These findings indicate that SV release was less synchronous in
210 *Rac1*$^{-/-}$ in a time- and frequency-dependent manner.

211 Taken together, we found that *Rac1*$^{-/-}$ had longer EPSC onsets and decreased EPSC
212 synchronicity, especially at high stimulation frequencies. Therefore, we conclude that the increase
213 of synaptic strength in *Rac1*$^{-/-}$ calyces is not due to changes in positional priming that result in
214 tighter SV coupling since tighter coupling would lead to shorter EPSC onset delays and higher
215 synchronicity in the *Rac1*$^{-/-}$ calyces.

216 **Loss of Rac1 facilitates EPSC and RRP recovery**

217 Modulation of molecular priming steps regulates RRP recovery (Neher and Brose, 2018;
218 Ritzau-Jost et al., 2018). Since Rac1 deletion increased SV fusogenicity and P_r throughout the
219 stimulus train, we hypothesized that RRP recovery was faster in the absence of Rac1. To test how
220 the loss of Rac1 influences RRP recovery, we carried afferent fiber stimulation using a paired train
221 protocol consisting of a 500 Hz depleting train (50 APs) followed by a second 500 Hz test train at
222 varying recovery intervals (Fig. 5). Recovery was then measured for both single EPSCs and the
223 RRP. For single EPSC recovery, we measured both absolute and fractional recovery by
224 normalizing the $EPSC_1$ amplitude of the test train to the $EPSC_1$ amplitude of the control train
225 relative to steady-state EPSC amplitudes. Recovery of $EPSC_1$ was significantly faster in *Rac1*$^{-/-}$
226 compared to *Rac1*$^{+/+}$ for both absolute and fractional recovery (absolute: *Rac1*$^{+/+}$ τ_w = 2.4 s vs
227 *Rac1*$^{-/-}$ τ_w = 1.7 s, p = 1e-12; fractional: *Rac1*$^{+/+}$ τ_w = 1.8 s vs *Rac1*$^{-/-}$ τ_w = 1.3 s, p = 3.2e-8,
228 n = 15/15, Fig. 5A). Next, we analyzed fractional RRP recovery by dividing the RRP estimate of
229 the test train by the RRP estimate of the depleting train and found that RRP recovery rates were
230 about 40% faster in *Rac1*$^{-/-}$ (*Rac1*$^{+/+}$ τ_w = 1.14 s vs *Rac1*$^{-/-}$ τ_w = 0.7 s, p = 1.1e-9, n = 15/15; Fig 5B).
231 Finally, we calculated the paired-pulse ratios ($EPSC_2/EPSC_1$) of the test train to estimate release

232 probability as a function of recovery interval. Independent of recovery interval, PPR was
233 consistently lower in *Rac1*$^{-/-}$ (Fig. 5C), consistent with the increased initial and steady-state P_r.

234 **Loss of Rac1 impacts delay and temporal precision of AP firing in response to SAM stimuli**

235 Animal vocalization including human speech is characterized by rapid amplitude
236 modulations (Joris et al., 2004). These amplitude modulations can be mimicked by sinusoidal
237 amplitude-modulated stimuli (SAM) which will produce periodic fluctuations in the firing rates of
238 the calyx of Held (Mc Laughlin et al., 2008; Tolnai et al., 2008). Therefore, different SAM
239 frequencies will differentially stress SV release and recovery mechanisms and can be used to
240 relate the observed changes in synaptic strength and SV recovery to potential impacts on auditory
241 signaling in the *Rac1*$^{-/-}$ calyces. Using *in vivo* responses to SAM stimuli (Tolnai et al., 2008) which
242 contained modulation frequencies between 20 Hz and 2000 Hz as templates for afferent fiber
243 stimulation, we recorded postsynaptic APs in loose-patch configuration (Fig. 6). First, we analyzed
244 how successful a presynaptic stimulus resulted in a postsynaptic AP to assess the reliability of
245 synaptic transmission and found no difference between *Rac1*$^{+/+}$ and *Rac1*$^{-/-}$ independent of
246 modulation frequency (Fig. 6B1). Since temporal precision is crucial in auditory signaling, we then
247 analyzed if the loss of Rac1 impacted the temporal precision of AP generation by calculating the
248 standard deviation of AP delays (AP jitter). Independent of modulation frequency, temporal
249 precision was unchanged when analyzed for the complete stimulus (Fig. 6B2). However, the
250 previous analysis showed that EPSC onset delay and synchronicity were only affected at high
251 stimulation frequencies. Since the SAM stimuli generate periods of high firing activity interspersed
252 with periods of low activity, we tested how preceding activity influenced AP jitter and AP delay.
253 First, we used the preceding interspike interval (ISI) as an estimate of preceding activity and
254 calculated AP jitter and AP delay for different ISIs (Fig. 6C1). Both, AP jitter and AP delay were
255 comparable between *Rac1*$^{+/+}$ and *Rac1*$^{-/-}$ for most ISIs but AP delay in *Rac1*$^{-/-}$ increased slightly at
256 short ISIs. Previous studies showed that EPSC/EPSP amplitudes, and subsequent AP generation,
257 are influenced by preceding neuronal activity (Haustein et al., 2008; Englitz et al., 2009; Lorteije

258 et al., 2009; Sonntag et al., 2011; Yang and Xu-Friedman, 2015; Ghanbari et al., 2020). Since our
259 previous analysis only considered the last ISI and thus is an incomplete estimate of preceding
260 activity, we estimated activity levels by calculating the sum of all preceding APs weighted by their
261 distance to the AP under observation (Fig. 6C2). Using this method, we found that AP jitter was
262 similar between *Rac1*$^{+/+}$ and *Rac1*$^{-/-}$ for low to moderate activity levels but diverged at increasing
263 activity levels with *Rac1*$^{-/-}$ showing higher AP jitter (*Rac1*$^{+/+}$ = 65 ± 32 µs vs. *Rac1*$^{-/-}$ = 99 ± 62 µs,
264 p = 1.5e-5 µs, n = 14/18). Similarly, AP delays were similar for low activity levels, but increased
265 more in *Rac1*$^{-/-}$ with increasing activity (*Rac1*$^{+/+}$ = 110 ± 52 µs vs. *Rac1*$^{-/-}$ = 158 ± 101 µs,
266 p = 0.03). These data suggest that the activity-dependent increase in EPSC onset and reduction
267 in EPSC synchronicity in *Rac1*$^{-/-}$ at high stimulation frequencies translates into a small but
268 consistent increase in AP delays and AP jitter.

269 **Discussion**

270 By ablating *Rac1* at the calyx of Held after hearing onset, we identified the presynaptic
271 roles of *Rac1* in regulating synaptic transmission and plasticity in a native neuronal circuit. Based
272 on our data we conclude that presynaptic Rac1 is a key regulator of synaptic strength and RRP
273 replenishment through SV priming steps that control intrinsic SV P_r. Therefore, we propose that
274 presynaptic Rac1 is a critical regulator for encoding information by neuronal circuits.

275 ***Rac1* regulates P_r and RRP recovery**

276 Our finding that Rac1 is a negative regulator of P_r is in contrast with a recent study in
277 primary cultured hippocampal neurons that concluded presynaptic Rac1 does not regulate P_r
278 (O'neil et al., 2021). Multiple reasons may explain these differences. One cause may be due to
279 the specific conditions of a native neuronal circuit that are not replicated in *in vitro* cultured
280 neuronal circuits. We specifically abated *Rac1* at a distinct developmental time point, two days
281 after hearing onset where neuronal circuit properties are well defined and the calyx of Held is
282 functionally mature (Englitz et al., 2009; Sonntag et al., 2009, 2011; Borst and Soria Van Hoeve,
283 2012). Although *Rac1* was ablated at 10 days *in vitro* (O'neil et al., 2021), the corresponding
284 developmental stage to *in vivo* hippocampal neurons is unclear. In addition, it is unknown to what
285 extent the artificial *in vitro* circuit properties determine synaptic transmission and plasticity
286 characteristics. Another critical difference between our studies was the recording condition. We
287 used 1.2 mM $[Ca^{2+}]_{ext}$ and physiological temperatures to mimic *in vivo* conditions (Lorteije et al.,
288 2009; Borst, 2010; Forsberg et al., 2019), while 2 mM $[Ca^{2+}]_{ext}$ at room temperature was used in
289 the prior study. As a result, we observed an initial P_r ~0.1 with no P_r higher than 0.15 in *Rac1*$^{+/+}$
290 calyces and a two-fold increase following Rac1 ablation. However, in the cultured neurons, the
291 initial P_r was ~0.4 in *Rac1*$^{+/+}$ with many values exceeding 0.5 in both excitatory and inhibitory
292 neurons. Therefore, it is likely that in cultured neurons, P_r was close to maximum or at maximum
293 thereby masking any potential increases in P_r in *Rac1*$^{-/-}$ neurons. In addition, many regulatory
294 steps in the SV lifecycle that influence P_r are temperature-dependent (Chanaday and Kavalali,

295 2020), and in mouse hippocampal synapses actin-dependent synaptic release enhancement was
296 only detected at physiological temperatures (Jensen et al., 2007).

297 The RRP size is a critical determinant of synaptic strength that maintains synaptic
298 transmission during ongoing stimulation. Since the RRP size varies with stimulation rates
299 (Thanawala and Regehr, 2013, 2016; Neher, 2015), SV replenishment is key in regulating RRP
300 size. SV replenishment rates are typically estimated by two methods (Hallermann and Silver,
301 2013; Neher, 2015): i) SV replenishment rates during ongoing stimulation which corresponds to
302 the slope of the line fit using the SMN plot, or ii) RRP replenishment rates that are estimated by
303 plotting the fraction of recovered RRP or initial ESPC amplitudes as a function of interstimulus
304 intervals following RRP depletion. Subsequently, the RRP replenishment rates are described by
305 the time constants of fits. Using the slope of the line fit, we found that *Rac1*$^{-/-}$ calyces had faster
306 SV replenishment rates and larger steady-state EPSC amplitudes at 50 Hz train stimulation which
307 is similar to observations in primary hippocampal cultures at 20 and 40 Hz train stimulation (O'neil
308 et al., 2021). In contrast, at 500 Hz train stimulation, there was no difference between *Rac1*$^{+/+}$ and
309 *Rac1*$^{-/-}$ calyces in SV replenishment rates or steady-state EPSC amplitudes. However, RRP
310 replenishment was best fit with a bi-exponential fit, with a faster slow component in *Rac1*$^{-/-}$ (1.8s
311 vs 2.4s), but no difference in fast component (~40 ms) or relative contribution of each time
312 constant. These observations run counter to numerous observations demonstrating that
313 increasing activity rates results in faster SV replenishment and shorter RRP recovery time
314 constants (Wang and Kaczmarek, 1998; Hallermann and Silver, 2013). However, the fractional
315 recovery in *Rac1*$^{-/-}$ calyces at 50 ms recovery interval was ~ 2 fold higher and steady-state EPSC
316 levels were similar at 500 Hz and larger at 50 Hz stimulation frequency despite increased depletion
317 in *Rac1*$^{-/-}$ calyces. Therefore, if defined as fractional recovery of the initial RRP rather than ongoing
318 SV replenishment during stimulation this would indicate faster SV replenishment rates in *Rac1*$^{-/-}$
319 calyces at 500 Hz stimulation frequency.

320 Replenishment rates depend on the release site vacancy which depends on P_r, therefore
321 P_r is critical in controlling SV replenishment (Vere-Jones, 1966; Quastel, 1997; Scheuss and
322 Neher, 2001a; Zucker and Regehr, 2002; Neher, 2010; Pulido and Marty, 2017; Kusick et al.,
323 2020; Tanaka et al., 2021). Analysis of steady-state P_r by two independent methods demonstrated
324 that the steady-state P_r was elevated in *Rac1*$^{-/-}$ calyces. Since the interstimulus intervals at both
325 50 Hz (20 ms) and 500 Hz (2 ms) stimulation frequency are shorter than the fast RRP
326 replenishment time constant, this indicates that Rac1 regulation of P_r controls SV replenishment
327 on the time scale of hundreds of microseconds which is faster than known SV recruitment steps.
328 To explain our conclusion, we assume two synapses with different P_r (*Rac1*$^{+/+}$ with 0.1 and *Rac1*$^{-}$
329 $^{/-}$ with 0.2) and steady-state RRP size (*Rac1*$^{+/+}$ with 20 SVs and *Rac1*$^{-/-}$ with 10 SVs), but similar
330 steady-state EPSCs during ongoing stimulation (500 Hz condition). In this scenario, both synapses
331 would replenish the same absolute number of SV, since each synapse will release 2 SVs per
332 stimulus (20*0.1 vs. 10*0.2) and these 2 SVs will be replenished between stimuli. Therefore, when
333 calculating the SV replenishment rate relative to total RRP at rest using back extrapolation, the
334 SV replenishment rates would be similar as the absolute replenishment and total RRP are the
335 same. However, if one defines SV replenishment as the proportion of the steady-state RRP
336 relative to the initial RRP, then the high-P_r synapse would have higher SV replenishment rates
337 compared to the low P_r synapse (20 % of the steady-state RRP vs. 10% of the steady-state RRP).
338 In contrast, at 50 Hz stimulation condition, steady-state EPSCs were larger in the high P_r (*Rac1*$^{-/-}$
339 *)* compared to low P_r synapse (*Rac1*$^{+/+}$*).* Assuming a similar steady-state RRP (e.g. 20 SVs), the
340 high P_r synapses would release and replenish more SVs per stimulus compared to the low P_r
341 synapse (0.1*20 = 2 SVs vs. 0.2*20 = 4 SVs). Therefore, the SV replenishment rate calculated
342 using back extrapolation will be faster in the high P_r synapse although the total RRP is the same.

343 **Rac1 regulation of SV Priming control SV P_r and RRP recovery**

344 In response to APs, synapse P_r is regulated by SV fusogenecity, the fusion willingness of
345 an SV (intrinsic SV P_r), and the localization of SVs relative to VGCCs (Schneggenburger and

346 Rosenmund, 2015). SV priming controls SV P_r through two steps, molecular priming and positional
347 priming (Neher and Brose, 2018). Molecular priming controls intrinsic SV P_r by regulating SV
348 fusogenicity through SV docking states which represent the conversion from loose-state (LS) to
349 tight-state (TS) and the tightness of the TS state (Neher and Brose, 2018). Positional priming
350 regulates the proximity of SVs to VGCCs to control SV P_r independent of intrinsic SV P_r (Neher,
351 2010). Based on our findings of how the loss of Rac1 impacted mEPSCs rates and AP-evoked
352 release, we propose that Rac1 regulates SV P_r and RRP recovery at the level of molecular priming.
353 Since mEPSCs are independent of VGCCs (Kavalali, 2015, 2020) they function as readouts of
354 molecular priming, with increased mEPSC rates corresponding to increased SV fusogenecity
355 (Basu et al., 2007; Schotten et al., 2015; Dong et al., 2018). In the absence of Rac1, mESPC rates
356 were increased in the presence of Cd^{2+} which rules out any Cav2.1 channel contribution.
357 Furthermore, the increase in SV P_r in *Rac1*$^{-/-}$ was not caused by changes in SV docking or RRP
358 size since both AZ ultrastructure and initial RRP size measured by AP train stimulation was
359 unchanged.
360 AP-evoked EPSCs in *Rac1*$^{-/-}$ calyces were delayed and less synchronous particularly at high firing
361 rates indicating that SVs were less tightly coupled in *Rac1*$^{-/-}$ calyces. The EPSC onset delay which
362 is an estimate of positional priming includes two components: conduction delay, the time from
363 afferent fiber stimulation to the presynaptic AP, and SV release delay, the time between
364 presynaptic AP and the onset of the EPSC which is mainly dependent on the distance between
365 SVs to VGCCs (Fedchyshyn and Wang, 2007). Since Rac1 regulates actin dynamics, the loss of
366 Rac1 may prolong conduction delay during train stimuli that obscured Rac1's role in positional
367 priming. If the conduction delay was solely responsible for the increase in onset delays, AP-evoked
368 release kinetics would be unchanged. However, both onset delay and release synchronicity were
369 activity-dependent in *Rac1*$^{-/-}$ calyces suggesting a change in SV release kinetics. Since after
370 hearing onset, the calyx of Held utilizes nanodomain release which targets SVs within ~25 nm of

371 the Cav2.1 channels (Fedchyshyn and Wang, 2005; Chen et al., 2015), the decrease in SV
372 release synchronicity suggests that more distal SVs were released in Rac1$^{-/-}$.

373 Another plausible scenario is that presynaptic APs in *Rac1*$^{-/-}$ were broader and contributed
374 to increased P_r. However, using TEA, a Kv3 channel blocker, to broaden the presynaptic AP
375 impairs high-frequency firing at the calyx of Held (Wang and Kaczmarek, 1998; Wang et al., 1998;
376 Johnston et al., 2010). Furthermore, presynaptic deletion of Kv3.3 channels broadens APs and
377 increased P_r but enhanced short-term depression and decreased steady-state EPSC amplitudes
378 (Richardson et al., 2022). Since *Rac1*$^{-/-}$ had similar or larger steady-state EPSCs, were able to
379 follow high-frequency stimulation, and the intrinsic SV fusogenicity *Rac1*$^{-/-}$ was increased, it is
380 unlikely that broadened APs contributed to increased P_r.

381 Loss of Rac1 might impact endocytosis through changes in actin signaling (Wu and Chan,
382 2022). However, at the calyx of Held, the endocytic role of F-actin appears to be negligible as actin
383 depolymerization using latrunculin did not affect endocytosis (Eguchi et al., 2017; Babu et al.,
384 2020). Furthermore, endocytosis acts on a time scale of seconds and would be too slow to
385 contribute to SV replenishment during train stimulation (Armbruster and Ryan, 2011). Although
386 ultrafast endocytosis occurs on a timescale of tens of milliseconds, it is F-actin dependent, and
387 SV reformation is too slow as it takes tens of seconds (Watanabe et al., 2013a, 2013b). In addition,
388 endocytosis is postulated to play a role in release site clearance (Neher, 2010)as the perturbation
389 of endocytosis increases the rate of synaptic depression and slows RRP recovery (Hua et al.,
390 2013) which we did not observe in the *Rac1*$^{-/-}$ calyces.

391 F-actin is implicated in the regulation of several SV life cycle steps which could impact SV
392 replenishment rates (Morales et al., 2000; Sakaba and Neher, 2003; Cingolani and Goda, 2008;
393 Waites et al., 2011; Lee et al., 2012, 2013; Montesinos et al., 2015; Rust and Maritzen, 2015,
394 2015). Specifically, F-actin has been proposed to act as a physical barrier within the presynaptic
395 AZ (Cingolani and Goda, 2008) as the transient application of latrunculin increased P_r and mEPSC
396 rates (Morales et al., 2000). Studies in which Septin 5 (Yang et al., 2010) or the actin cytoskeleton

397 was disrupted (Lee et al., 2012) are in support of the idea of F-actin as a structural barrier
398 impacting positional priming. However, F-action may act as a vertical barrier to impact molecular
399 priming (Yang et al., 2010). Therefore, since Rac1 regulates molecular priming, we propose that
400 Rac1's regulation of F-actin acts as a vertical barrier to regulate the conversion from LS to TS and
401 the tightness of the TS (Fig. 7). In our model, the loss of Rac1 results in local actin
402 depolymerization in the AZ which increases SV fusogenicity by placing SVs in closer proximity to
403 the AZ which increases the LS to TS transition rate and TS tightening which increases P_r. In
404 support of our model, increased P_r has been demonstrated to correlate with shortened tethering
405 filaments that resulted in SVs positioned more closely to the presynaptic membrane (Jung et al.,
406 2021). Since GIT proteins (Montesinos et al., 2015), Arp2/3 (O'neil et al., 2021), and Piccolo
407 (Waites et al., 2011) are regulators of F-actin dynamics and control P_r this suggests that F-actin
408 signaling cascades at the AZ regulate P_r potentially through molecular priming and/or positional
409 priming. More importantly, this suggests that molecules regulating F-actin dynamics at the AZ
410 could be key regulators of SV replenishment independent of facilitation sensors.

411 **Rac1 regulation of auditory signaling and information processing.**

412 The ability to accurately encode sound information requires synaptic transmission in the
413 lower auditory brainstem to drive and sustain precise AP firing over rapid and large fluctuations of
414 AP firing rates up to the kilohertz range (Grothe et al., 2010; Borst and Soria Van Hoeve, 2012;
415 Friauf et al., 2015). The calyx of Held/MNTB synapse is a safe and reliable synaptic relay that
416 transforms afferent AP spike patterns from the cochlear nucleus (CN) into precisely timed
417 inhibition to several mono- and binaural cell groups (Spirou et al., 1990; Scheuss and Neher,
418 2001b; Joris et al., 2004; Englitz et al., 2009; Lorteije et al., 2009; Sonntag et al., 2011). The use
419 of SAM stimuli which mimics the neuronal response to environmental sounds (Joris et al., 2004;
420 Tolnai et al., 2008) suggests that loss of Rac1 did not deteriorate the faithful auditory signaling
421 properties over different amplitude modulation frequencies. However, we found that the increase
422 in EPSC onset and decrease in SV release synchronicity in *Rac1*$^{-/-}$ translated into larger AP delay

423 and AP jitter at high activity levels. Although the absolute changes were modest, the need for
424 immaculate temporal precision in the auditory brainstem might cause a more severe impact in
425 downstream nuclei such as the lateral and medial superior olive. Since the calyx of Held generates
426 suprathreshold EPSCs even under short-term depression (Lorteije et al., 2009; Lorteije and Borst,
427 2011), the impact of P_r changes caused by Rac1 ablation will be modest in affecting MNTB firing,
428 but likely more substantial in other synapses in the SPON, MSO, or LSO that operate close to AP
429 threshold or rely on synaptic integration to encode information.

430 Mutations in Rac1 that result in loss or gain of function are associated with intellectual
431 disability (Reijnders et al., 2017; Zamboni et al., 2018). While much attention has focused on Rac1
432 dysregulation in the dendritic compartment or neuronal development, our work demonstrates that
433 presynaptic loss of Rac1 increases P_r independent of its developmental role. Therefore, human
434 mutations in Rac1 might affect P_r and excitation-inhibition balance and thereby alter plasticity in
435 many different neuronal circuits associated with neurological disorders and addiction (Dietz et al.,
436 2012; Bai et al., 2015; Wright et al., 2020).

437 **Methods**

438 **Animals**

439 All experiments were performed following animal welfare laws and approved by the Institutional
440 Committee for Care and Use of Animals at the University of Iowa (PHS Assurance No. D16-00009
441 (A3021-01) (Animal Protocol 0021952) and complied with accepted ethical best practices. Animals
442 were housed at a 12-hour light/dark cycle and had access to food and water ad libitum.
443 Experiments were performed on Rac1^{tm1Djk} (*Rac1*$^{fl/fl}$) mice (Glogauer et al., 2003;
444 RRID:IMSR_JAX: 005550, The Jackson Laboratory, Bar Harbor, USA) of either sex. Animals of
445 this line possess a *loxP* site flanking exon 1 of the *Rac1* gene disrupting Rac1 expression after
446 recombination mediated by Cre recombinase. Genotyping was performed using PCR-
447 amplification with the following primers 5'-TCC AAT CTG TGC TGC CCA TC-3' and 5'-GAT GCT
448 TCT AGG GGT GAG CC-3' and amplification products (*Rac1*$^{fl/fl}$: 242 bp, wildtype: 115 bp) were
449 separated gel electrophoresis on a 1.5% agarose gel (Glogauer et al., 2003). Viral vectors were
450 injected at postnatal day 14 (P14) and experiments were performed at P28-30. All available
451 measures were taken to minimize animal pain and suffering.

452 **DNA construct and recombinant viral vector production**

453 Helper-dependent adenoviral vectors (HdAd) expressing a codon-optimized Cre recombinase
454 (Cre) (Shimshek et al., 2002) were produced as previously described (Montesinos et al., 2016;
455 Lübbert et al., 2017). These HdAd vectors contain two independent transgene cassettes that
456 independently express Cre recombinase and EGFP or myristoylated EGFP (mEGFP) under the
457 control of 470 bp human synapsin promoter (Lübbert et al., 2017). In brief, the expression cassette
458 with Cre recombinase was cloned into the pdelta28E4 SynEGFP plasmid using the *Asc*I enzyme
459 digestion site. The final plasmid has been modified to also contain a separate EGFP or
460 myristoylated EGFP (mEGFP) expression cassette. Then, the pHAD plasmid was linearized by
461 *PmeI* enzyme to expose the ends of the 5' and 3' inverted terminal repeats (ITRs) and transfected
462 into 116 producer cells (Profection® Mammalian Transfection System, Promega, Madison, WI,

463 USA). Helper virus (HV) was added the following day for HdAd production. Forty-eight hours
464 postinfection, after cytopathic effects have taken place, cells were subjected to three freeze/thaw
465 cycles for lysis and release of the viral particles. HdAd was purified by CsCl ultracentrifugation.
466 HdAd was stored at -80 °C in storage buffer (10 mM HEPES, 1 mM $MgCl_2$, 250 mM sucrose, pH
467 7.4).

468 **Virus injections**

469 Virus injections at P14 were performed as previously described (Lübbert et al., 2019). Briefly, mice
470 were anesthetized with 5% isoflurane inhalation and anesthesia was maintained with 2%
471 isoflurane throughout the procedure. Subcutaneous injection of physiological saline, lidocaine,
472 bupivacaine, and meloxicam was used to treat loss of liquid and alleviate pain. The injection site
473 was determined using the Stereodrive software (Neurostar) and corrected for head orientation and
474 tilt. A small hole (diameter <1 mm) was drilled into the skull using a foot-pedal controlled drill MH-
475 170 (Foredom). The virus solution was injected via a glass pipet (Drummond) at a rate of 100
476 nL/min with a nanoliter injector (NanoW, Neurostar). Following the injection, the glass needle was
477 left in place for 1 min to dissipate the pressure and then slowly retracted. Animals were then placed
478 under an infrared heat lamp and allowed to recover before being returned to their respective cages
479 with their mother.

480 **Confocal imaging and reconstruction of presynaptic terminals**

481 For reconstruction of the calyx of Held terminals, animals were injected with viral vectors
482 expressing either mEGFP (yielding *Rac1*$^{+/+}$) or Cre recombinase and mEGFP (yielding *Rac1*$^{-/-}$).
483 Mice were anesthetized with an intraperitoneal injection of tribromoethanol (250 mg/kg body
484 weight) and transcardially perfused with ice-cold 0.1 M phosphate buffer (PB, pH 7.4) followed by
485 4% paraformaldehyde (PFA) in 0.1 M PB. Brains were removed and post-fixed overnight in 4%
486 PFA solution at 4°C. The next day, brains were sliced into 40 µm sections on a Leica VT1200
487 vibratome. mEGFP positive slices were identified and mounted on cover slips with Aqua
488 Polymount (Polysciences, Inc., Warrington, PA, USA). Confocal images were acquired with a

489 Zeiss LSM 700 or 880 confocal scanning microscope using a 63x/1.3 NA Apochromat multi-
490 immersion objective. Image stacks were collected using 0.44 um plane line scans with line
491 average of four times. Images were processed using Fiji (Schindelin et al., 2012, http://fiji.sc.,
492 RRID:SCR 002285). Calyx reconstructions were performed blind to genotype using Imaris
493 Measurement Pro (BitPlane) using automatic signal detection manual curation in single planes in
494 Z-stack confocal images as previously described (Radulovic et al., 2020).

495 **Electron Microscopy**

496 Preembedding immuno-electron microscopy was performed as previously described (Montesinos
497 et al., 2015; Dong et al., 2018). Briefly, *Rac*$^{fl/fl}$ mice injected at P14 with HdAd co-expressing Cre-
498 recombinase and EGFP were anesthetized and perfused transcardially at P28 with phosphate-
499 buffered saline (PBS, 150 mM NaCl, 25 mM Sørensen's phosphate buffer, pH 7.4) followed by
500 fixative solution for 7-9 min containing 4% PFA, 0.5% glutaraldehyde, and 0.2% picric acid in 100
501 mM Sørensen's phosphate buffer (PB, pH 7.4). Brains were post-fixed with 4% PFA in PB
502 overnight and 50-µm coronal sections of the brainstem were obtained on a vibratome (Leica
503 VT1200S). Expression of EGFP at the calyx of Held terminals was visualized using an
504 epifluorescence inverted microscope (CKX41, Olympus) equipped with an XCite Series 120Q
505 lamp (Excelitas Technologies), and only those samples showing EGFP were further processed.
506 After washing with PB, sections were cryoprotected with 10%, 20%, and 30% sucrose in PB and
507 submersed into liquid nitrogen, then thawed. Sections were incubated in a blocking solution
508 containing 10% normal goat serum (NGS), 1% fish skin gelatin (FSG), in 50 mM Tris-buffered
509 saline (TBS, 150 mM NaCl, 50 mM Tris, pH 7.4) for 1h, and incubated with an anti-GFP antibody
510 (0.1µg/ml, ab6556, Abcam, RRID: AB_305564) diluted in TBS containing 1% NGS, 0.1% FSG
511 plus 0.05% NaN_3 at 4°C for 48h. After washing with TBS, sections were incubated overnight in
512 nanogold conjugated goat anti-rabbit IgG (1:100, Jackson Immunoresearch, RRID: AB_2340585)
513 diluted in TBS containing 1% NGS and 0.1% FSG. Immunogold-labeled sections were washed in
514 PBS, briefly fixed with 1% glutaraldehyde in PBS, and silver intensified using an HQ silver

515 intensification kit (Nanoprobe). After washing with PB, sections were treated with 0.5% OsO_4 in
516 0.1M PB for 20 min, en-bloc stained with 1% uranyl acetate, dehydrated and flat embedded in
517 Durcupan resin (Sigma-Aldrich). After trimming out the MNTB region, ultrathin sections were
518 prepared with 40 nm-thickness using an ultramicrotome (EM UC7, Leica). Sections were
519 counterstained with uranyl acetate and lead citrate and examined in a Tecnai G2 Spirit BioTwin
520 transmission electron microscope (Thermo Fisher Scientific) at 100 kV acceleration voltage.
521 Images were taken with a Veleta CCD camera (Olympus) operated by TIA software (Thermo
522 Fisher Scientific). Images used for quantification were taken at 60 000x magnification.

523 **TEM image analysis**

524 Calyces positive for Cre expression (*Rac1*$^{-/-}$) were identified by immunogold labeling with an anti-
525 GFP antibody and compared to EGFP-negative terminals (*Rac1*$^{+/+}$) in the same slice or calyces in
526 the wildtype sample. All TEM data were analyzed using Fiji imaging analysis software (Schindelin
527 et al., 2012). Each presynaptic active zone (AZ) was defined as the membrane directly opposing
528 the postsynaptic density, and the length of each AZ was measured. Vesicles within 200 nm from
529 each AZ were manually selected and their distances relative to the AZ were calculated using a
530 32-bit Euclidean distance map generated from the AZ. For data analysis, vesicle distances were
531 binned every 5 nm and counted (Montesinos et al., 2015; Dong et al., 2018). Vesicles less than 5
532 nm from the AZ were considered “docked”. Three animals for each condition and ~40 AZs per
533 animal were analyzed. Analysis was performed blind to genotype independently by three
534 researchers and results were averaged.

535 **Electrophysiology**

536 Acute coronal brainstem slices (~200 µm) containing the MNTB were prepared as previously
537 described (Chen et al., 2013; Thomas et al., 2019). Briefly, after decapitation of the animal, the
538 brain was immersed in low-calcium artificial cerebrospinal fluid (aCSF) solution containing (in mM):
539 125 NaCl, 2.5 KCl, 3 $MgCl_2$, 0.1 $CaCl_2$, 10 glucose, 25 $NaHCO_3$, 1.25 NaH_2PO_4, 0.4 L-ascorbic
540 acid, 3 myo-inositol, and 2 Na-pyruvate, pH 7.3–7.4). Brain slices were obtained using a Leica VT

541 1200S vibratome equipped with zirconia ceramic blades (EF-INZ10, Cadence Blades) as
542 previously described. The blade was advanced at a speed of 20-50 µm/s. Slices were immediately
543 transferred to an incubation beaker containing standard extracellular solution (same as above but
544 using 1 mM $MgCl_2$ and 1.2 mM $CaCl_2$) at ~37°C and continuously bubbled with 95% O_2–5% CO_2.
545 After approximately 45 min of incubation, slices were transferred to a recording chamber with the
546 same saline solution at physiological temperature (~37°C).
547 Electrical stimulation of afferent fibers was performed as previously described (Forsythe and
548 Barnes-Davies, 1993a, 1993b). Briefly, a bipolar platinum-iridium electrode was positioned
549 medially of the MNTB to stimulate afferent fibers (FHC, Model MX214EP). Postsynaptic MNTB
550 neurons were whole-cell voltage-clamped at −60 mV using an EPC10/2 amplifier controlled by
551 Patchmaster Software (version 2x90.2, HEKA Elektronik, RRID:SCR_000034). Slices were
552 continuously perfused with normal aCSF solution at a rate of 1 mL/min and visualized by an
553 upright microscope (BX51WI, Olympus) through a 60x water-immersion objective (LUMPlanFL N,
554 Olympus) and an EMCCD camera (Andor Luca S, Oxford Instruments). To identify calyces
555 expressing Cre-recombinase and EGFP, the slice was illuminated at an excitation wavelength of
556 480 nm using a Polychrome V xenon bulb monochromator (TILL Photonics). For whole-cell
557 voltage-clamp recordings, the standard extracellular solution was supplemented with 1 mM
558 kynurenic acid to avoid saturation of postsynaptic AMPA receptors, 50 µM D-AP-5 to block NMDA
559 receptors, and 20 µM bicuculline and 5 µM strychnine to block inhibitory GABA- and glycine
560 receptors, respectively (all Tocris Bioscience). Patch pipettes had a resistance of ∼3–4 MΩ and
561 were filled with the following (in mM): 130 Cs-gluconate, 20 tetraethylammonium (TEA)-Cl, 10
562 HEPES, 5 Na_2-phosphocreatine, 4 Mg-ATP, 0.3 Na-GTP, 6 QX-314, and 5 EGTA, pH 7.2 (315
563 mOsm. Reported voltages are uncorrected for a calculated liquid junction potential of 13 mV. For
564 loose-patch recordings, the extracellular solution was supplemented with 20 µM bicuculline and
565 5 µM strychnine, and the patch pipettes were filled with aCSF. To simulate *in vivo* activity levels,

566 afferent fibers were stimulated with activity patterns previously recorded *in vivo* in response to
567 sinusoidal amplitude-modulated (SAM) sound stimulation (Tolnai et al., 2008).

568 mEPSCs were recorded with the same aCSF supplemented with 50 mM D-AP5, 20 μM
569 bicuculline, 5 μM strychnine, 1 μM TTX, and 20 mM TEA. In a subset of *Rac1*$^{-/-}$ recordings, Cd^{2+}
570 (cadmium chloride), a non-selective Ca^{2+} channel blocker was flushed in during recordings to
571 determine the impact of VGCC on spontaneous SV release. The baseline mEPSC frequency was
572 established by recording each cell for at least one minute before Cd^{2+} was flushed in via the bath
573 perfusion. MNTB principal neurons were whole-cell voltage-clamped at -80 mV and recorded until
574 enough mEPSCs (>25) were recorded. Overlapping events were excluded from the analysis.

575 Data were acquired at a sampling rate of 100 kHz and lowpass filtered at 6 kHz. Series resistance
576 (3–8 MΩ) was compensated online to <3 MΩ, except for mEPSC recordings where series
577 resistance (<9 MΩ) was not compensated. All experiments were performed at near-physiological
578 temperature (36-37°C) and the temperature was maintained by a heated bath chamber (HCS,
579 ALA Scientific Instruments) and perfusion system (HPC-2, ALA Scientific Instruments). The
580 temperature of the bath solution was monitored during the experiment using a glass-coated micro
581 thermistor.

582 **Electrophysiological data analysis**

583 Electrophysiological data were imported to Matlab (version 9.10; The Mathworks,
584 RRID:SCR_001622) using a custom-modified version of sigTool (Lidierth, 2009) and Igor Pro
585 (version 8.0.4.2, Wavemetrics, RRID:SCR_000325) equipped with Patcher's Power Tools
586 (version 2.19, RRID:SCR_001950) and NeuroMatic (Rothman and Silver, 2018,
587 RRID:SCR_004186), and analyzed offline with custom-written functions in Matlab and IgorPro.
588 The remaining series resistance was compensated offline to 0 MΩ with a time lag of 10 μs
589 (Traynelis, 1998). EPSC amplitudes were measured as peak amplitude minus baseline preceding
590 the EPSC. RRP size and P_r were calculated using the EQ method (Elmqvist and Quastel, 1965),

591 back-extrapolation method (SMN with correction, Neher, 2015), and NpRf model (Thanawala and
592 Regehr, 2016) as previously described (Lübbert et al., 2019). Steady-state Pr was calculated by
593 dividing the steady-state EPSC by the RRP size corrected for partial depletion: $Pr_{ss} =$
594 $EPSC_{ss}/(RRP \cdot EPSC_{ss}/EPSC_1)$. Onset time of EPSCs was determined by fitting a Boltzmann
595 function to the EPSC rising flank and calculating the time point of maximum curvature, as
596 described previously (Fedchyshyn and Wang, 2007). The duration between stimulus and EPSC
597 onset was defined as EPSC onset delay. Synchronicity of SV release was estimated for individual
598 EPSCs by dividing their EPSC amplitude by their EPSC charge.

599 Recordings of mEPSCs were analyzed using NeuroMatic in Igor Pro. Potential events were
600 detected when exceeding an amplitude threshold at 4-6 times the standard deviation of the
601 baseline and all events were manually curated to exclude false positives. Rise time was measured
602 between 10% and 90% of the amplitude. Full-width at half-maximal amplitude (FWHM) was
603 measured at 50% amplitude.

604 $$A\left(1 - e^{-\frac{t}{\tau_r}}\right)\left(Fe^{-\frac{t}{\tau_{d1}}} + (1-F)e^{-\frac{t}{\tau_{d2}}}\right)$$

605 Amplitudes and rise and decay time of mEPSCs were derived from the fit. Overlapping events
606 were first deconvolved with a template mEPSC to determine their onset and then fit as a linear
607 sum of multi-exponential equations.
608 Recovery of SVs was estimated by non-linear least-square fits for single EPSC and RRP recovery.
609 Both types of recovery were best fit with a bi-exponential function of the form:

610 $$A\left(1 - f\left(e^{-\frac{t}{\tau_{d1}}}\right) + (1-f)\left(e^{-\frac{t}{\tau_{d2}}}\right)\right)$$

611 with variable A constraint to 1 when fitting fractional recovery. An F-test was used to statistically
612 determine the better fit as described previously. Fractional recovery of the first EPSC was
613 calculated as $(EPSC_{test}^{1} - EPSC_{dep}^{ss})/(EPSC_{dep}^{1} - EPSC_{dep}^{ss})$ where $EPSC_{test}^{1}$ is the amplitude of the

first EPSC of the test train, $EPSC_{dep}^{ss}$ the steady-state amplitude of the depleting train and $EPSC_{dep}^{1}$ the amplitude of the first EPSC of the depleting train.

To estimate preceding neuronal activity during SAM stimulation, we calculated the interspike interval (ISI) as the distance to the preceding AP. For the analysis of AP responses during SAM stimulation, we used the preceding ISI to estimate the influence of previous activity during SAM recordings. Since short-term plasticity can extend well beyond the last ISI, we also estimated preceding activity by calculating the sum of all preceding events with each event weighted by its distance to the AP under observation. This weighting was implemented as a single-exponential decaying function, emphasizing temporally close events over more distant ones (Sonntag et al., 2009; Keine et al., 2016). The time constant was set to 30 ms, consistent with previous reports (Yang and Xu-Friedman, 2015). The calculation was also performed with time constants of 10 ms and 100 ms yielding similar results.

Experimental Design and Statistical analysis

For the electrophysiological data analysis and morphological reconstruction, individual neurons were considered independent samples. For thin-section TEM analysis, AZs were considered independent samples (244 total AZs, 6 animals, ~40 AZs each). Statistical analysis was conducted in MATLAB (version 9.4, RRID:SCR_001622) and GraphPad Prism (RRID:SCR_002798). Data distributions were tested for Gaussianity using the Shapiro-Wilk test. To compare two groups, a two-tailed unpaired Student's t-test with Welch's correction (normal distribution) or a two-tailed Mann-Whitney *U* test (non-normal distribution) was used. Fits to data were subject to F-tests to determine the better model (mono- or biexponential) and for comparison between groups. For interpretation of all statistical tests, a p-value of 0.05 was deemed significant. Effect sizes were calculated using the MES toolbox in MATLAB (Hentschke and Stüttgen, 2011) and are reported as Cohen's U_1 for two-sample comparison and eta-squared (η^2) for RM ANOVA. No statistical test was performed to pre-determine sample sizes. Exact p-values, test statistics, and effect sizes for all statistical comparisons are summarized in Table 1. Boxplots in the figures show median,

640 interquartile, and minimum/maximum within 1.5 times the interquartile range. Average data in the
641 text are reported as mean ± standard deviation.

642 **Data and Software Accessibility**

643 All experimental data and custom-written software central to the conclusion of this study are
644 available at http://dx.doi.org/10.17632/c4b7gn8bh7 under the terms of the Creative Commons
645 Attribution 4.0 License (CC BY 4.0).

Acknowledgments

We would like to thank the members of the Young lab for their comments on the manuscript. This work was supported by the National Institute of Deafness and Other Communication Disorders (R01 DC014093) National Institute of Neurological Disorders and Stroke (R01NS110742), the University of Iowa (SMY), and a German Research Foundation postdoctoral fellowship (DFG 420075000) (CK).

Competing interests

The authors declare no competing interests.

654 **References**

655 Alabi ARA, Tsien RW (2012) Synaptic vesicle pools and dynamics. Cold Spring Harb Perspect
656 Biol 4:a013680–a013680.

657 Armbruster M, Ryan TA (2011) Synaptic vesicle retrieval time is a cell-wide rather than individual-
658 synapse property. Nat Neurosci 14:824–826.

659 Azarfar A, Calcini N, Huang C, Zeldenrust F, Celikel T (2018) Neural coding: A single neuron's
660 perspective. Neurosci Biobehav Rev 94:238–247.

661 Babu LPA, Wang HY, Eguchi K, Guillaud L, Takahashi T (2020) Microtubule and actin differentially
662 regulate synaptic vesicle cycling to maintain high-frequency neurotransmission. J Neurosci
663 40:131–142.

664 Bai Y, Xiang X, Liang C, Shi L (2015) Regulating Rac in the nervous system: Molecular function
665 and disease implication of Rac GEFs and GAPs. Biomed Res Int 2015:632450.

666 Basu J, Betz A, Brose N, Rosenmund C (2007) Munc13-1 C1 Domain Activation Lowers the
667 Energy Barrier for Synaptic Vesicle Fusion. J Neurosci 27:1200–1210.

668 Bleckert A, Photowala H, Alford S (2012) Dual pools of actin at presynaptic terminals. J
669 Neurophysiol 107:3479–3492.

670 Bonnycastle K, Davenport EC, Cousin MA (2021) Presynaptic dysfunction in neurodevelopmental
671 disorders: Insights from the synaptic vesicle life cycle. J Neurochem 157:179–207.

672 Borst JGG (2010) The low synaptic release probability in vivo. Trends Neurosci 33:259–266.

673 Borst JGG, Soria Van Hoeve J (2012) The calyx of held synapse: From model synapse to auditory
674 relay. Annu Rev Physiol 74:199–224.

675 Bosco EE, Mulloy JC, Zheng Y (2009) Rac1 GTPase: A "Rac" of all trades. Cell Mol Life Sci
676 66:370–374.

677 Brette R (2015) Philosophy of the spike: Rate-based vs. Spike-based theories of the brain. Front
678 Syst Neurosci 9:151.

679 Chanaday NL, Kavalali ET (2020) Is Ca2+ Essential for Synaptic Vesicle Endocytosis? Trends
680 Neurosci 43:77–79.

681 Chen Z, Cooper B, Kalla S, Varoqueaux F, Young SM (2013) The munc13 proteins differentially
682 regulate readily releasable pool dynamics and calcium-dependent recovery at a central
683 synapse. J Neurosci 33:8336–8351.

684 Chen Z, Das B, Nakamura Y, DiGregorio DA, Young SM, Nakamura XY, DiGregorio DA, Young
685 SM (2015) Ca2+ Channel to Synaptic Vesicle Distance Accounts for the Readily Releasable
686 Pool Kinetics at a Functionally Mature Auditory Synapse. J Neurosci 35:2083–2100.

687 Cingolani LA, Goda Y (2008) Actin in action: The interplay between the actin cytoskeleton and
688 synaptic efficacy. Nat Rev Neurosci 9:344–356.

689 Cole JC, Villa BRS, Wilkinson RS (2000) Disruption of actin impedes transmitter release in snake
690 motor terminals. J Physiol 525 Pt 3:579–586.

691 Crins TTHH, Rusu SI, Rodríguez-Contreras A, Borst JGG (2011) Developmental changes in short-
692 term plasticity at the rat calyx of Held synapse. J Neurosci 31:11706–11717.

693 Dietz DM et al. (2012) Rac1 is essential in cocaine-induced structural plasticity of nucleus
694 accumbens neurons. Nat Neurosci 15:891–896.

695 Dong W, Radulovic T, Goral RO, Thomas C, Suarez Montesinos M, Guerrero-Given D, Hagiwara
696 A, Putzke T, Hida Y, Abe M, Sakimura K, Kamasawa N, Ohtsuka T, Young SM (2018)
697 CAST/ELKS Proteins Control Voltage-Gated Ca 2+ Channel Density and Synaptic Release
698 Probability at a Mammalian Central Synapse. Cell Rep 24:284-293.e6.

699 Doussau F, Gasman S, Humeau Y, Vitiello F, Popoff M, Boquet P, Bader MF, Poulain B (2000) A

700 Rho-related GTPase is involved in Ca2+-dependent neurotransmitter exocytosis. J Biol
701 Chem 275:7764–7770.

702 Eggermann E, Bucurenciu I, Goswami SP, Jonas P (2012) Nanodomain coupling between Ca^{2+}
703 channels and sensors of exocytosis at fast mammalian synapses. Nat Rev Neurosci 13:7–
704 21.

705 Eguchi K, Taoufiq Z, Thorn-Seshold O, Trauner D, Hasegawa M, Takahashi T (2017) Wild-Type
706 Monomeric α-Synuclein Can Impair Vesicle Endocytosis and Synaptic Fidelity via Tubulin
707 Polymerization at the Calyx of Held. J Neurosci 37:6043–6052.

708 Elmqvist D, Quastel DM (1965) A quantitative study of end-plate potentials in isolated human
709 muscle. J Physiol 178:505–529.

710 Englitz B, Tolnai S, Typlt M, Jost J, Rübsamen R (2009) Reliability of synaptic transmission at the
711 synapses of held in vivo under acoustic stimulation. PLoS One 4:e7014.

712 Fedchyshyn MJ, Wang L-Y (2007) Activity-dependent changes in temporal components of
713 neurotransmission at the juvenile mouse calyx of Held synapse. J Physiol 581:581–602.

714 Fedchyshyn MJ, Wang LY (2005) Developmental transformation of the release modality at the
715 calyx of held synapse. J Neurosci 25:4131–4140.

716 Forsberg M, Seth H, Björefeldt A, Lyckenvik T, Andersson M, Wasling P, Zetterberg H, Hanse E
717 (2019) Ionized calcium in human cerebrospinal fluid and its influence on intrinsic and synaptic
718 excitability of hippocampal pyramidal neurons in the rat. J Neurochem 149:452–470.

719 Forsythe ID, Barnes-Davies M (1993a) The binaural auditory pathway: Excitatory amino acid
720 receptors mediate dual timecourse excitatory postsynaptic currents in the rat medial nucleus
721 of the trapezoid body. Proc R Soc B Biol Sci 251:151–157.

722 Forsythe ID, Barnes-Davies M (1993b) The binaural auditory pathway: Membrane currents limiting

723 multiple action potential generation in the rat medial nucleus of the trapezoid body. Proc R
724 Soc B Biol Sci 251:143–150.

725 Friauf E, Fischer AU, Fuhr MF (2015) Synaptic plasticity in the auditory system: a review. Cell
726 Tissue Res 361:177–213.

727 Gentile JE, Carrizales MG, Koleske AJ (2022) Control of Synapse Structure and Function by Actin
728 and Its Regulators. Cells 11:603.

729 Ghanbari A, Ren N, Keine C, Stoelzel C, Englitz B, Swadlow HA, Stevenson IH (2020) Modeling
730 the short-term dynamics of in vivo excitatory spike transmission. J Neurosci 40:4185–4202.

731 Glogauer M, Marchal CC, Zhu F, Worku A, Clausen BE, Foerster I, Marks P, Downey GP, Dinauer
732 M, Kwiatkowski DJ (2003) Rac1 Deletion in Mouse Neutrophils Has Selective Effects on
733 Neutrophil Functions. J Immunol 170:5652–5657.

734 Grothe B, Pecka M, McAlpine D (2010) Mechanisms of sound localization in mammals. Physiol
735 Rev 90:983–1012.

736 Hallermann S, Silver RA (2013) Sustaining rapid vesicular release at active zones: Potential roles
737 for vesicle tethering. Trends Neurosci 36:185–194.

738 Haustein MD, Reinert T, Warnatsch A, Englitz B, Dietz B, Robitzki A, R??bsamen R, Milenkovic
739 I, Rübsamen R, Milenkovic I (2008) Synaptic transmission and short-term plasticity at the
740 calyx of Held synapse revealed by multielectrode array recordings. J Neurosci Methods
741 174:227–236.

742 Hentschke H, Stüttgen MC (2011) Computation of measures of effect size for neuroscience data
743 sets. Eur J Neurosci 34:1887–1894.

744 Hua Y, Woehler A, Kahms M, Haucke V, Neher E, Klingauf J (2013) Blocking endocytosis
745 enhances short-term synaptic depression under conditions of normal availability of vesicles.

Neuron 80:343–349.

Iwasaki S, Momiyama A, Uchitel OD, Takahashi T (2000) Developmental changes in calcium channel types mediating central synaptic transmission. J Neurosci 20:59–65.

Iwasaki S, Takahashi T (1998) Developmental changes in calcium channel types mediating synaptic transmission in rat auditory brainstem. J Physiol 509 (Pt 2:419–423.

Iwasaki S, Takahashi T (2001) Developmental regulation of transmitter release at the calyx of Held in rat auditory brainstem. J Physiol 534:861–871.

Jensen TP, Filoteo AG, Knopfel T, Empson RM (2007) Presynaptic plasma membrane Ca2+ ATPase isoform 2a regulates excitatory synaptic transmission in rat hippocampal CA3. J Physiol 579:85–99.

Johnston J, Forsythe ID, Kopp-Scheinpflug C (2010) Going native: Voltage-gated potassium channels controlling neuronal excitability. J Physiol 588:3187–3200.

Joris PX, Schreiner CE, Rees A (2004) Neural Processing of Amplitude-Modulated Sounds. Physiol Rev 84:541–577.

Joris PX, Trussell LO (2018) The Calyx of Held: A Hypothesis on the Need for Reliable Timing in an Intensity-Difference Encoder. Neuron 100:534–549.

Jung JH, Kirk LM, Bourne JN, Harris KM (2021) Shortened tethering filaments stabilize presynaptic vesicles in support of elevated release probability during LTP in rat hippocampus. Proc Natl Acad Sci U S A 118:1–8.

Kaeser PS, Regehr WG (2014) Molecular mechanisms for synchronous, asynchronous, and spontaneous neurotransmitter release. Annu Rev Physiol 76:333–363.

Kavalali ET (2015) The mechanisms and functions of spontaneous neurotransmitter release. Nat Rev Neurosci 16:5–16.

769 Kavalali ET (2020) Neuronal Ca2+ signalling at rest and during spontaneous neurotransmission.
770 J Physiol 598:1649–1654.

771 Keine C, Rübsamen R, Englitz B (2016) Inhibition in the auditory brainstem enhances signal
772 representation and regulates gain in complex acoustic environments. Elife 5:19295.

773 Klug A, Borst JGG, Carlson BA, Kopp-Scheinpflug C, Klyachko VA, Xu-Friedman MA (2012) How
774 Do Short-Term Changes at Synapses Fine-Tune Information Processing? J Neurosci
775 32:14058–14063.

776 Kumanogoh H, Miyata S, Sokawa Y, Maekawa S (2001) Biochemical and morphological analysis
777 on the localization of Rac1 in neurons. Neurosci Res 39:189–196.

778 Kusick GF, Chin M, Raychaudhuri S, Lippmann K, Adula KP, Hujber EJ, Vu T, Davis MW,
779 Jorgensen EM, Watanabe S (2020) Synaptic vesicles transiently dock to refill release sites.
780 Nat Neurosci 23:1329–1338.

781 Lee JS, Ho W-KK, Lee S-HH (2012) Actin-dependent rapid recruitment of reluctant synaptic
782 vesicles into a fast-releasing vesicle pool. Proc Natl Acad Sci U S A 109:E765-74.

783 Lee JS, Ho W-KK, Neher E, Lee S-HH (2013) Superpriming of synaptic vesicles after their
784 recruitment to the readily releasable pool. Proc Natl Acad Sci U S A 110:15079–15084.

785 Lidierth M (2009) sigTOOL: A MATLAB-based environment for sharing laboratory-developed
786 software to analyze biological signals. J Neurosci Methods 178:188–196.

787 Lorteije JAM, Borst JGG (2011) Contribution of the mouse calyx of Held synapse to tone
788 adaptation. Eur J Neurosci 33:251–258.

789 Lorteije JAM, Rusu SI, Kushmerick C, Borst JGG (2009) Reliability and precision of the mouse
790 calyx of Held synapse. J Neurosci 29:13770–13784.

791 Lübbert M, Goral RO, Keine C, Thomas C, Guerrero-Given D, Putzke T, Satterfield R, Kamasawa

792 N, Young SM (2019) CaV2.1 α1 Subunit Expression Regulates Presynaptic CaV2.1
793 Abundance and Synaptic Strength at a Central Synapse. Neuron 101:260-273.e6.

794 Lübbert M, Goral RO, Satterfield R, Putzke T, van den Maagdenberg AM, Kamasawa N, Young
795 SM (2017) A novel region in the Ca V 2.1 α 1 subunit C-terminus regulates fast synaptic
796 vesicle fusion and vesicle docking at the mammalian presynaptic active zone. Elife 6:1–22.

797 Mc Laughlin M, Van Der Heijden M, Joris PX (2008) How secure is in vivo synaptic transmission
798 at the calyx of Held? J Neurosci 28:10206–10219.

799 Miki T, Malagon G, Pulido C, Llano I, Neher E, Marty A, Correspondence AM, Marty A (2016)
800 Actin- and Myosin-Dependent Vesicle Loading of Presynaptic Docking Sites Prior to
801 Exocytosis. Neuron 91:808–823.

802 Montesinos MS, Dong W, Goff K, Das B, Guerrero-Given D, Schmalzigaug R, Premont RT,
803 Satterfield R, Kamasawa N, Young SM (2015) Presynaptic Deletion of GIT Proteins Results
804 in Increased Synaptic Strength at a Mammalian Central Synapse. Neuron 88:918–925.

805 Montesinos MS, Satterfield R, Young SM (2016) Helper-Dependent Adenoviral Vectors and Their
806 Use for Neuroscience Applications. In: High-Resolution Imaging of Cellular Proteins, pp 73–
807 90.

808 Morales M, Colicos MA, Goda Y (2000) Actin-Dependent Regulation of Neurotransmitter Release
809 at Central Synapses. Neuron 27:539–550.

810 Neher E (2010) What is rate-limiting during sustained synaptic activity: Vesicle supply or the
811 availability of release sites. Front Synaptic Neurosci 2:1–6.

812 Neher E (2015) Merits and Limitations of Vesicle Pool Models in View of Heterogeneous
813 Populations of Synaptic Vesicles. Neuron 87:1131–1142.

814 Neher E, Brose N (2018) Dynamically Primed Synaptic Vesicle States: Key to Understand

815 Synaptic Short-Term Plasticity. Neuron 100:1283–1291.

816 Neher E, Sakaba T (2008) Multiple Roles of Calcium Ions in the Regulation of Neurotransmitter
817 Release. Neuron 59:861–872.

818 O'neil SD, Rácz B, Brown WE, Gao Y, Soderblom EJ, Yasuda R, Soderling SH (2021) Action
819 potential-coupled rho gtpase signaling drives presynaptic plasticity. Elife 10:1–44.

820 Pulido C, Marty A (2017) Quantal fluctuations in central mammalian synapses: Functional role of
821 vesicular docking sites. Physiol Rev 97:1403–1430.

822 Quastel DMJ (1997) The binomial model in fluctuation analysis of quantal neurotransmitter
823 release. Biophys J 72:728–753.

824 Radulovic T, Dong W, Goral RO, Thomas CI, Veeraraghavan P, Montesinos MS, Guerrero-Given
825 D, Goff K, Lübbert M, Kamasawa N, Ohtsuka T, Young SM (2020) Presynaptic development
826 is controlled by the core active zone proteins CAST/ELKS. J Physiol 598:2431–2452.

827 Reijnders MRF et al. (2017) RAC1 Missense Mutations in Developmental Disorders with Diverse
828 Phenotypes. Am J Hum Genet 101:466–477.

829 Reinagel P, Laughlin S (2001) Natural stimulus statistics. Network 12:237–240.

830 Richardson A, Ciampani V, Stancu M, Bondarenko K, Newton S, Steinert JR, Pilati N, Graham
831 BP, Kopp-Scheinpflug C, Forsythe ID (2022) Kv3.3 subunits control presynaptic action
832 potential waveform and neurotransmitter release at a central excitatory synapse. Elife 11:1–
833 34.

834 Ritzau-Jost A, Jablonski L, Viotti J, Lipstein N, Eilers J, Hallermann S (2018) Apparent calcium
835 dependence of vesicle recruitment. J Physiol 596:4693–4707.

836 Rollenhagen A, Lübke JHRR (2006) The morphology of excitatory central synapses: From
837 structure to function. Cell Tissue Res 326:221–237.

838 Rothman JS, Silver RA (2018) Neuromatic: An integrated open-source software toolkit for
839 acquisition, analysis and simulation of electrophysiological data. Front Neuroinform 12:1–21.

840 Rust MB, Maritzen T (2015) Relevance of presynaptic actin dynamics for synapse function and
841 mouse behavior. Exp Cell Res 335:165–171.

842 Sakaba T (2006) Roles of the Fast-Releasing and the Slowly Releasing Vesicles in Synaptic
843 Transmission at the Calyx of Held. J Neurosci 26:5863–5871.

844 Sakaba T, Neher E (2003) Involvement of actin polymerization in vesicle recruitment at the calyx
845 of held synapse. J Neurosci 23:837–846.

846 Sätzler K, Söhl LF, Bollmann JH, Borst JGG, Frotscher M, Sakmann B, Lübke JHRR (2002) Three-
847 dimensional reconstruction of a calyx of Held and its postsynaptic principal neuron in the
848 medial nucleus of the trapezoid body. J Neurosci 22:10567–10579.

849 Scheuss V, Neher E (2001a) Estimating synaptic parameters from mean, variance, and
850 covariance in trains of synaptic responses. Biophys J 81:1970–1989.

851 Scheuss V, Neher E (2001b) Estimating synaptic parameters from mean, variance, and
852 covariance in trains of synaptic responses. Biophys J 81:1970–1989.

853 Schindelin J, Arganda-Carreras I, Frise E, Kaynig V, Longair M, Pietzsch T, Preibisch S, Rueden
854 C, Saalfeld S, Schmid B, Tinevez JY, White DJ, Hartenstein V, Eliceiri K, Tomancak P,
855 Cardona A (2012) Fiji: An open-source platform for biological-image analysis. Nat Methods
856 9:676–682.

857 Schneggenburger R, Rosenmund C (2015) Molecular mechanisms governing Ca(2+) regulation
858 of evoked and spontaneous release. Nat Neurosci 18:935–941.

859 Schotten S, Meijer M, Walter AM, Huson V, Mamer L, Kalogreades L, Ter Veer M, Ruiter M, Brose
860 N, Rosenmund C, Sørensen JB, Verhage M, Cornelisse LN (2015) Additive effects on the

861 energy barrier for synaptic vesicle fusion cause supralinear effects on the vesicle fusion rate.
862 Elife 2015:1–25.

863 Shimshek DR, Kim J, Hübner MR, Spergel DJ, Buchholz F, Casanova E, Stewart AF, Seeburg
864 PH, Sprengel R (2002) Codon-improved Cre recombinase (iCre) expression in the mouse.
865 Genesis 32:19–26.

866 Sonntag M, Englitz B, Kopp-Scheinpflug C, Rübsamen R (2009) Early postnatal development of
867 spontaneous and acoustically evoked discharge activity of principal cells of the medial
868 nucleus of the trapezoid body: An in vivo study in mice. J Neurosci 29:9510–9520.

869 Sonntag M, Englitz B, Typlt M, Rübsamen R (2011) The calyx of Held develops adult-like
870 dynamics and reliability by hearing onset in the mouse in vivo. J Neurosci 31:6699–6709.

871 Spirou GA, Brownell WE, Zidanic M (1990) Recordings from cat trapezoid body and HRP labeling
872 of globular bushy cell axons. J Neurophysiol 63:1169–1190.

873 Tanaka M, Sakaba T, Miki T (2021) Quantal analysis estimates docking site occupancy
874 determining short-term depression at hippocampal glutamatergic synapses. J Physiol
875 599:5301–5327.

876 Taschenberger H, Leão RM, Rowland KC, Spirou GA, von Gersdorff H (2002) Optimizing synaptic
877 architecture and efficiency for high-frequency transmission. Neuron 36:1127–1143.

878 Thanawala MS, Regehr WG (2013) Presynaptic calcium influx controls neurotransmitter release
879 in part by regulating the effective size of the readily releasable pool. J Neurosci 33:4625–
880 4633.

881 Thanawala MS, Regehr WG (2016) Determining synaptic parameters using high-frequency
882 activation. J Neurosci Methods 264:136–152.

883 Theunissen FE, Elie JE (2014) Neural processing of natural sounds. Nat Rev Neurosci 15:355–

884 366.

885 Thomas CI, Keine C, Okayama S, Satterfield R, Musgrove M, Guerrero-Given D, Kamasawa N,
886 Young SM (2019) Presynaptic Mitochondria Volume and Abundance Increase during
887 Development of a High-Fidelity Synapse. J Neurosci 39:7994–8012.

888 Threadgill R, Bobb K, Ghosh A (1997) Regulation of dendritic growth and remodeling by Rho,
889 Rac, and Cdc42. Neuron 19:625–634.

890 Tolnai S, Hernandez O, Englitz B, Rübsamen R, Malmierca MS (2008) The medial nucleus of the
891 trapezoid body in rat: Spectral and temporal properties vary with anatomical location of the
892 units. Eur J Neurosci 27:2587–2598.

893 Torres VI, Vallejo D, Inestrosa NC (2017) Emerging Synaptic Molecules as Candidates in the
894 Etiology of Neurological Disorders. Neural Plast 2017.

895 Traynelis SF (1998) Software-based correction of single compartment series resistance errors. J
896 Neurosci Methods 86:25–34.

897 Vere-Jones D (1966) Simple Stochastic Models for the Release of Quanta of Transmitter From a
898 Nerve Terminal. Aust J Stat 8:53–63.

899 Waites CL, Garner CC (2011) Presynaptic function in health and disease. Trends Neurosci
900 34:326–337.

901 Waites CL, Leal-Ortiz S a., Andlauer TFMM, Sigrist SJ, Garner CC (2011) Piccolo regulates the
902 dynamic assembly of presynaptic F-actin. J Neurosci 31:14250–14263.

903 Wang LY, Gan L, Forsythe ID, Kaczmarek LK (1998) Contribution of the Kv3.1 potassium channel
904 to high frequency firing in mouse auditory neurones. J Physiol 509:183–194.

905 Wang LY, Kaczmarek LK (1998) High-frequency firing helps replenish the readily releasable pool
906 of synaptic vesicles. Nature 394:384–388.

907 Watanabe S, Liu Q, Davis MW, Hollopeter G, Thomas N, Jorgensen NB, Jorgensen EM (2013a)
908 Ultrafast endocytosis at Caenorhabditis elegans neuromuscular junctions. Elife 2013:1–24.

909 Watanabe S, Rost BR, Camacho-Pérez M, Davis MW, Söhl-Kielczynski B, Rosenmund C,
910 Jorgensen EM (2013b) Ultrafast endocytosis at mouse hippocampal synapses. Nature
911 504:242–247.

912 Wimmer VC, Horstmann H, Groh A, Kuner T (2006) Donut-like topology of synaptic vesicles with
913 a central cluster of mitochondria wrapped into membrane protrusions: a novel structure-
914 function module of the adult calyx of Held. J Neurosci 26:109–116.

915 Wondolowski J, Dickman D (2013) Emerging links between homeostatic synaptic plasticity and
916 neurological disease. Front Cell Neurosci 7:223.

917 Wright WJ, Graziane NM, Neumann PA, Hamilton PJ, Cates HM, Fuerst L, Spenceley A,
918 MacKinnon-Booth N, Iyer K, Huang YH, Shaham Y, Schlüter OM, Nestler EJ, Dong Y (2020)
919 Silent synapses dictate cocaine memory destabilization and reconsolidation. Nat Neurosci
920 23:32–46.

921 Wu L-GG, Chan CY (2022) Multiple Roles of Actin in Exo- and Endocytosis. Front Synaptic
922 Neurosci 14:1–13.

923 Xu Z, Chen Y (2019) Spatiotemporal regulation of rho gtpases in neuronal migration. Cells 8.

924 Xue M, Craig TK, Xu J, Chao HT, Rizo J, Rosenmund C (2010) Binding of the complexin N
925 terminus to the SNARE complex potentiates synaptic-vesicle fusogenicity. Nat Struct Mol Biol
926 17:568–575.

927 Yang H, Xu-Friedman MA (2015) Skipped-stimulus approach reveals that short-term plasticity
928 dominates synaptic strength during ongoing activity. J Neurosci 35:8297–8307.

929 Yang YM, Fedchyshyn MJ, Grande G, Aitoubah J, Tsang CW, Xie H, Ackerley CA, Trimble WS,

930 Wang LY (2010) Septins regulate developmental switching from microdomain to nanodomain
931 coupling of Ca2+ influx to neurotransmitter release at a central synapse. Neuron 67:100–
932 115.

933 Yasuda R (2017) Biophysics of Biochemical Signaling in Dendritic Spines: Implications in Synaptic
934 Plasticity. Biophys J 113:2152–2159.

935 Young SM, Neher E (2009) Synaptotagmin Has an Essential Function in Synaptic Vesicle
936 Positioning for Synchronous Release in Addition to Its Role as a Calcium Sensor. Neuron
937 63:482–496.

938 Zamboni V, Jones R, Umbach A, Ammoni A, Passafaro M, Hirsch E, Merlo GR (2018) Rho
939 GTPases in intellectual disability: From genetics to therapeutic opportunities. Int J Mol Sci
940 19:187–191.

941 Zhang H, Ben Zablah Y, Zhang H, Jia Z (2021) Rho Signaling in Synaptic Plasticity, Memory, and
942 Brain Disorders. Front Cell Dev Biol 9:729076.

943 Zucker RS, Regehr WG (2002) Short-term synaptic plasticity. Annu Rev Physiol 64:355–405.

944

945 **Figures**

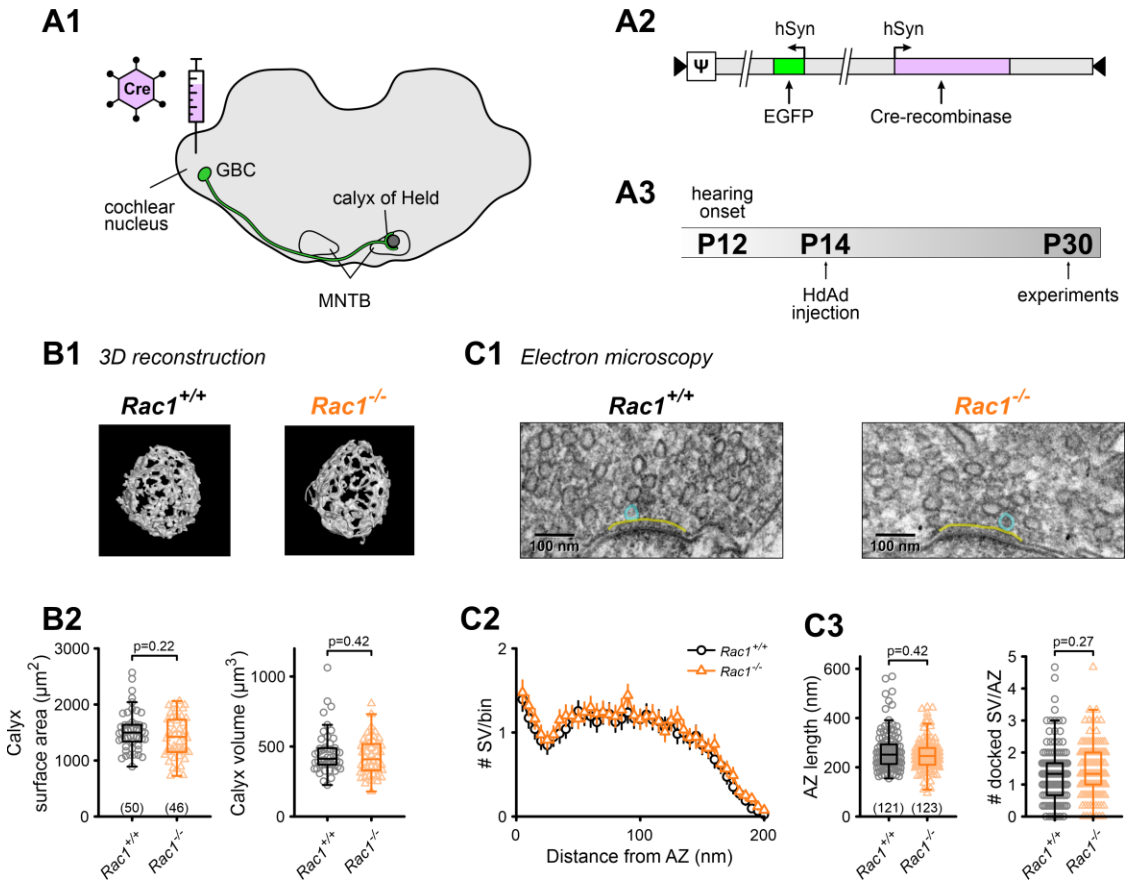

946

947 **Fig. 1: Loss of presynaptic Rac1 after hearing onset does not affect calyx of Held gross**
948 **morphology or ultrastructure**. (**A**) Cre recombinase-expressing HdAds were injected into the
949 cochlear nucleus of *Rac1*$^{fl/fl}$ mice at P14, yielding *Rac1*$^{-/-}$ calyces of Held. All experiments were
950 performed at around four weeks of age. Cre-recombinase-expressing calyces could be visually
951 identified by simultaneous expression of EGFP. (**B1**) Representative reconstruction of calyx
952 terminals of *Rac1*$^{+/+}$ (left) and *Rac1*$^{-/-}$ (right) animals. (**B2**) Calyx morphology assessed by surface
953 area (left) and volume (right) was not affected by the loss of Rac1 (**C1**) Representative EM images
954 of the active zone (yellow) and docked SV (blue) to assess synaptic ultrastructure. (**C2**) SV
955 distribution as a function of distance to AZ was not different between *Rac1*$^{+/+}$ and *Rac1*$^{-/-}$. (**C3**) AZ
956 length and number of docked SV were comparable between *Rac1*$^{+/+}$ *and Rac1*$^{-/-}$. Box plot whiskers
957 extend to the minimum/maximum within the 1.5 interquartile range; open markers indicate

958 individual data points. For EM data, the results of three independent investigators were averaged.

959 The results of statistical tests are summarized in Table 1.

960

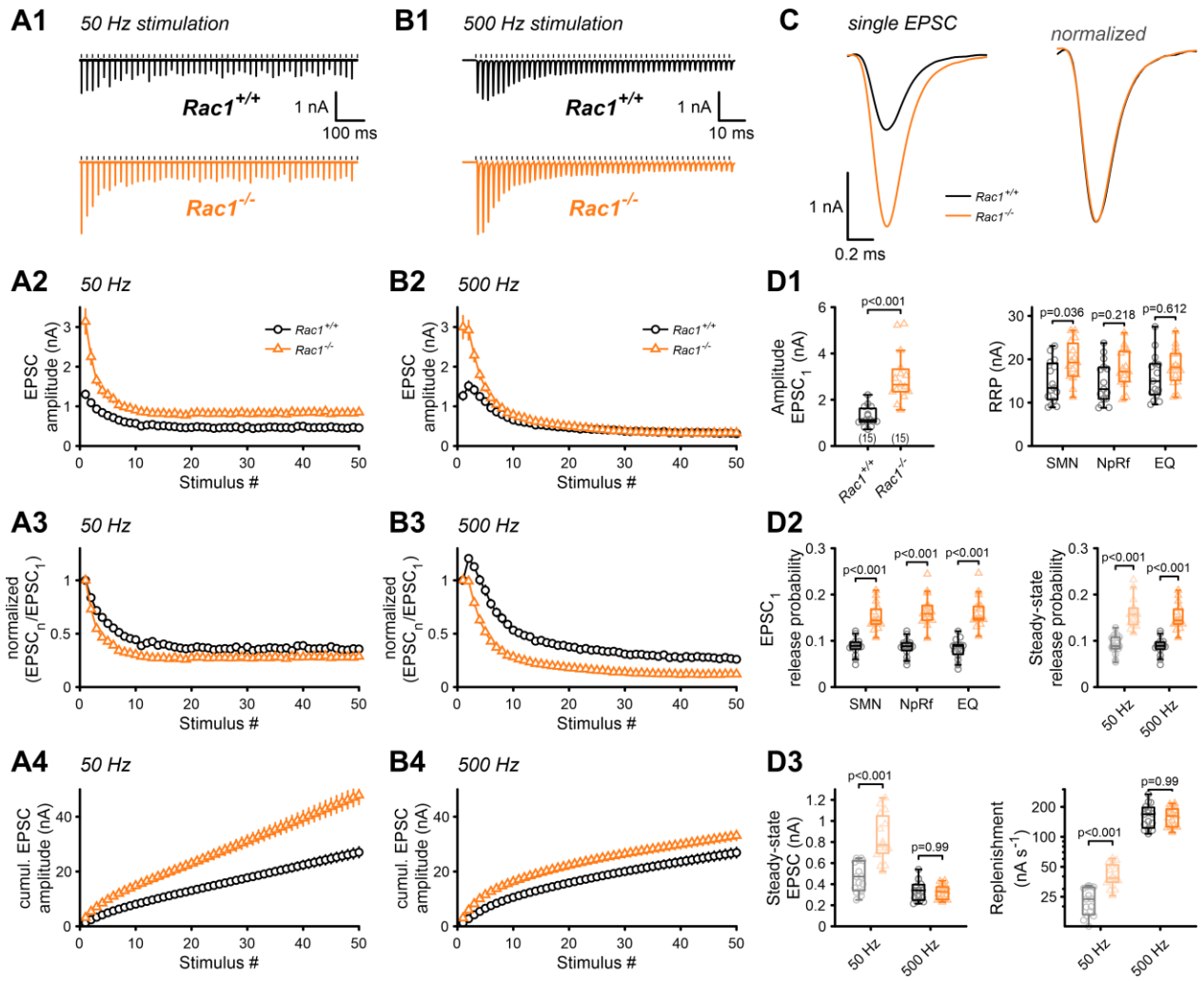

Fig. 2: Presynaptic Rac1 regulates synaptic vesicles release probability and synaptic strength. (**A**) Synaptic transmission at the calyx of Held – MNTB synapse was studied at P28 after deletion of Rac1 at P14 at different stimulation frequencies. (**A1, B1**) Representative evoked EPSCs for *Rac1*$^{+/+}$ (black) and *Rac1*$^{-/-}$ (orange) at 50 Hz and 500 Hz stimulation frequency and (**C1**) Magnification of the first EPSC. Ablation of presynaptic Rac1 resulted in increased EPSC amplitude with no change in EPSC dynamics (**A2-A4**) At 50 Hz stimulation frequency, *Rac1*$^{-/-}$ showed stronger short-term depression and larger steady-state EPSC amplitudes. (**B2-B4**) At 500 Hz stimulation frequency, loss of Rac1 resulted in a lack of short-term facilitation and increased synaptic depression with no change in steady-state EPSC amplitude (**D1**) Population data showing an increase in first EPSC amplitude in *Rac1*$^{-/-}$ with little or no change in RRP size

972 (**D2**) Population data for initial (left) and steady-state release probability (right) indicating that
973 release probability in *Rac1*$^{-/-}$ was elevated independent of estimation method and stimulation
974 frequency. (**D3**) Population data of steady-state EPSC amplitudes and replenishment rates at 50
975 and 500 Hz stimulation frequency. *Rac1*$^{-/-}$ had larger steady-state EPSCs and faster
976 replenishment at 50 Hz but not 500 Hz stimulation frequency. The results of statistical tests are
977 summarized in Table 1.

978

979

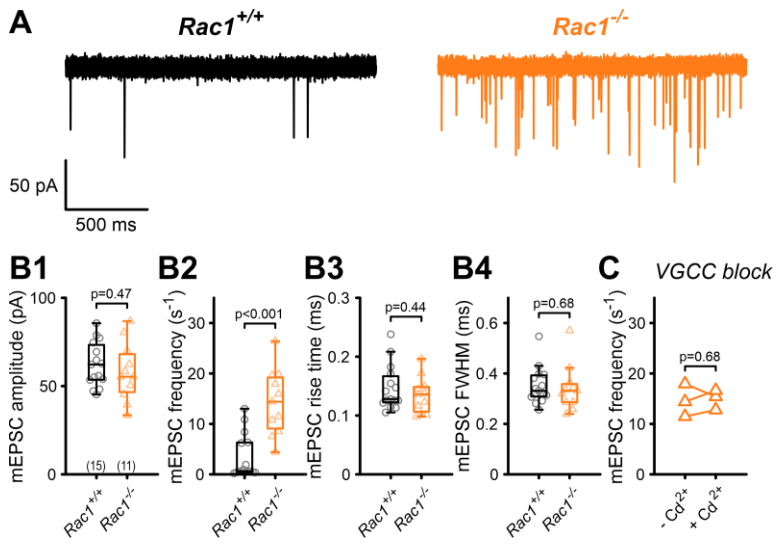

980 **Fig. 3: Presynaptic loss of Rac1 increase calcium-independent neurotransmitter release.**
981 (**A**) Representative recordings of mEPSCs for *Rac1*$^{+/+}$ (left, black) and *Rac1*$^{-/-}$ (right, orange). (**B1-**
982 **B4**) Rac1 deletion increased mEPSC frequency but did not affect mEPSC amplitude, rise time, or
983 full width at half-maximal amplitude (FWHM). (**C**) The increased mEPSC rates at *Rac1*$^{-/-}$ were
984 independent of presynaptic voltage-gated calcium channels (VGCC) as blocking VGCC with
985 cadmium (Cd^{2+}) did not affect mEPSC frequency. The results of statistical tests are summarized
986 in Table 1.

987

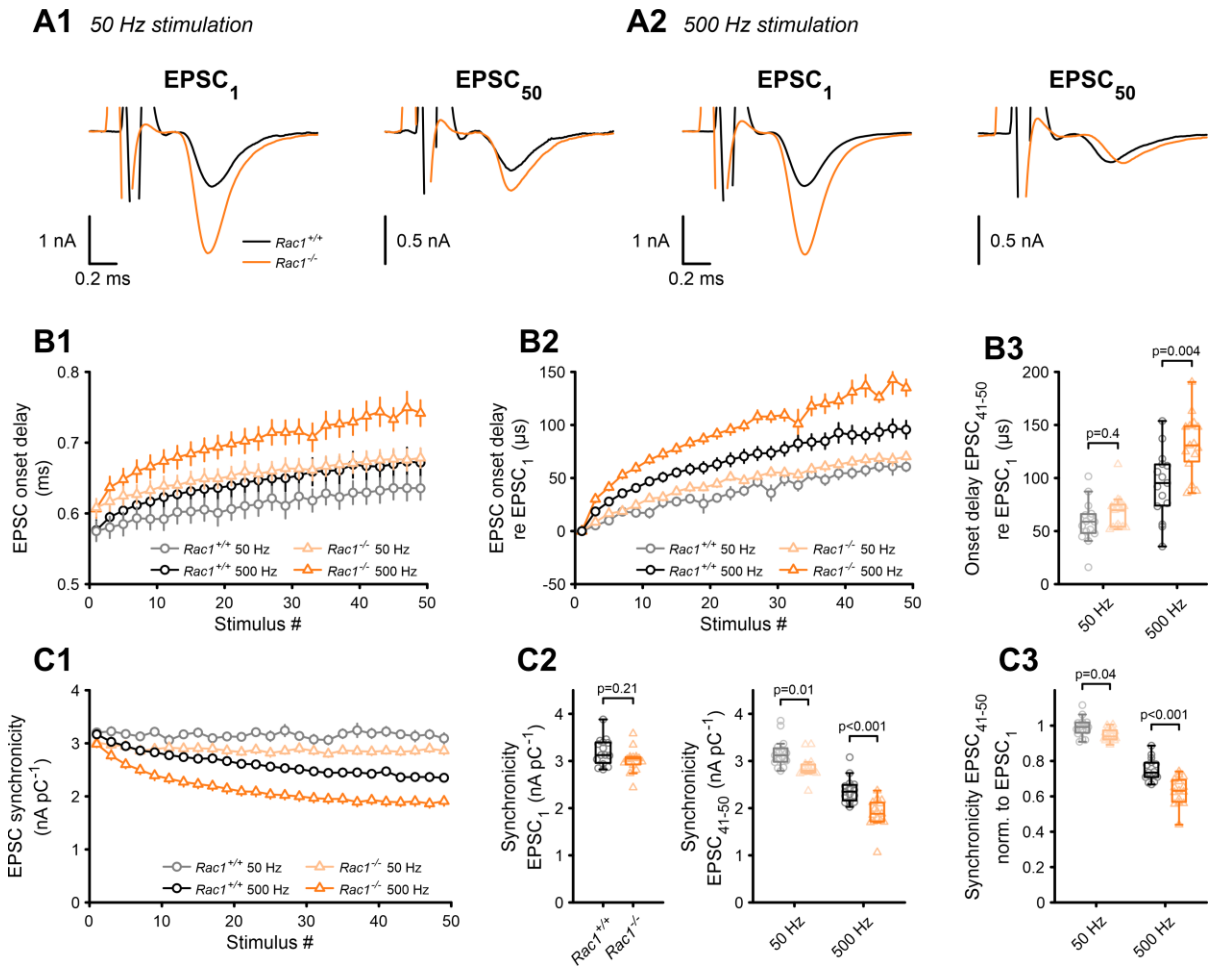

Fig. 4: Presynaptic loss of Rac1 decreases SV synchronicity and prolongs EPSC onset at high-frequency stimulation. (**A**) Experiments were performed at low (50 Hz, A1) and high (500 Hz, A2) stimulation frequencies. Representative recordings of first ($EPSC_1$) and last ($EPSC_{50}$) EPSC in the stimulus train. Traces are aligned at the EPSC onset of the first EPSC. Stimulus artifacts are partially blanked for better visibility. Note the shift in the onset of $EPSC_{50}$ in *Rac1*$^{-/-}$ at 500 Hz but not 50 Hz (**B1**) Absolute EPSC onset delay for 50 Hz (gray and light orange) and 500 Hz (black and orange) stimulation. (**B2**) EPSC onset delay relative to $EPSC_1$ for 50 Hz (gray and light orange) and 500 Hz (black and orange). At 50 Hz, the EPSC onset delay was similar between *Rac1*$^{+/+}$ and *Rac1*$^{-/-}$. At 500 Hz, the EPSC onset delay was substantially larger at *Rac1*$^{-/-}$. For better visualization, only every second data point is shown. (**B3**) EPSC onset delay of the last ten EPSCs relative to $EPSC_1$ for 50 Hz and 500 Hz stimulation. EPSC delay of the last

1000 ten EPSC was not different between *Rac1*$^{+/+}$ and *Rac1*$^{-/-}$ at 50 Hz but increased for *Rac1*$^{-/-}$ at
1001 500 Hz stimulation frequency. (**C1**) Analysis of EPSC synchronicity during 50 Hz and 500 Hz
1002 stimulation. Synchronicity was calculated by dividing the EPSC amplitudes by the EPSC charge.
1003 Note the more severe loss of EPSC synchronicity for *Rac1*$^{-/-}$ at 500 Hz stimulation. For better
1004 visualization only every second data point is shown (**C2**) EPSC synchronicity was not different for
1005 $EPSC_1$, but slightly reduced for *Rac1*$^{-/-}$ at 50 Hz and substantially lower at 500 Hz stimulation
1006 frequency. (**C3**) EPSC synchronicity of last ten EPSCs normalized to $EPSC_1$. Note the progressive
1007 loss of synchronicity in *Rac1*$^{-/-}$ with increasing stimulation frequency. The results of statistical tests
1008 are summarized in Table 1.

1009

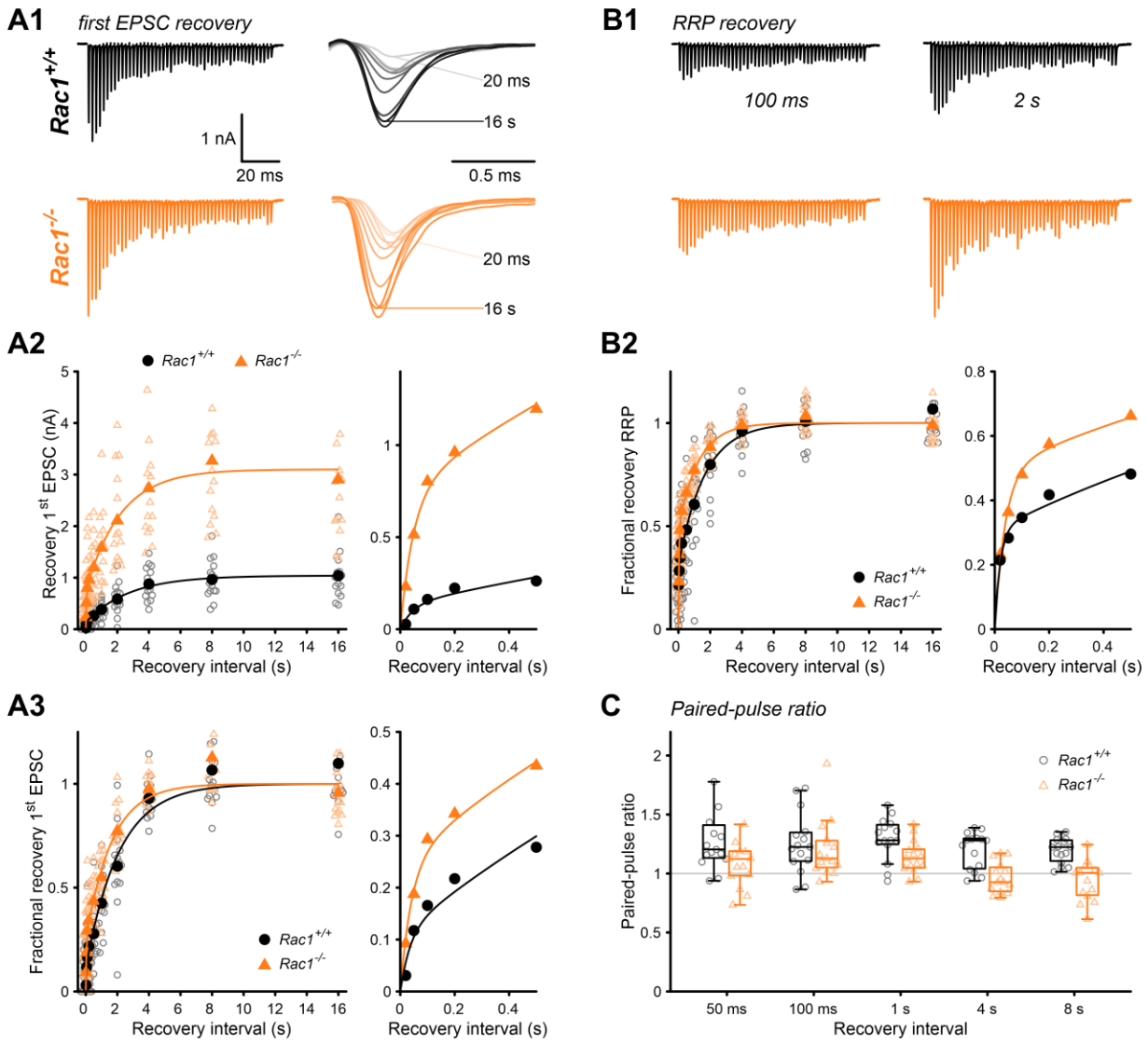

Fig. 5: Loss of presynaptic Rac1 facilitates synaptic vesicle recovery. (**A**) Recovery of single EPSC and RRP recovery was measured by two consecutive train stimuli (depleting stimulus and recovery stimulus) at 500 Hz at varying recovery intervals. (**A**) Single EPSC recovery. (**A1**) Representative traces for *Rac1*$^{+/+}$ (black) and *Rac1*$^{-/-}$ (orange) for recovery intervals ranging from 20 ms to 16 s. (**A2**) Recovery of absolute EPSC amplitudes as a function of recovery interval with magnification of short intervals (right). (**A3**) Fractional EPSC recovery as a function of recovery interval. (**B**) Recovery of the RRP (**B1**) Representative recovery traces after 100 ms and 2 s, the depleting stimulus train is the same as in A1. (**B2**) Fractional RRP recovery was faster in *Rac1*$^{-/-}$ compared to *Rac1*$^{+/+}$. (**B3**) Recovery of the paired-pulse ratio (PPR) of the first two EPSCs of the

1020 recovery train. PPR was consistently lower in *Rac1*$^{-/-}$ but the difference was emphasized at longer

1021 recovery intervals. The results of statistical tests are summarized in Table 1.

1022

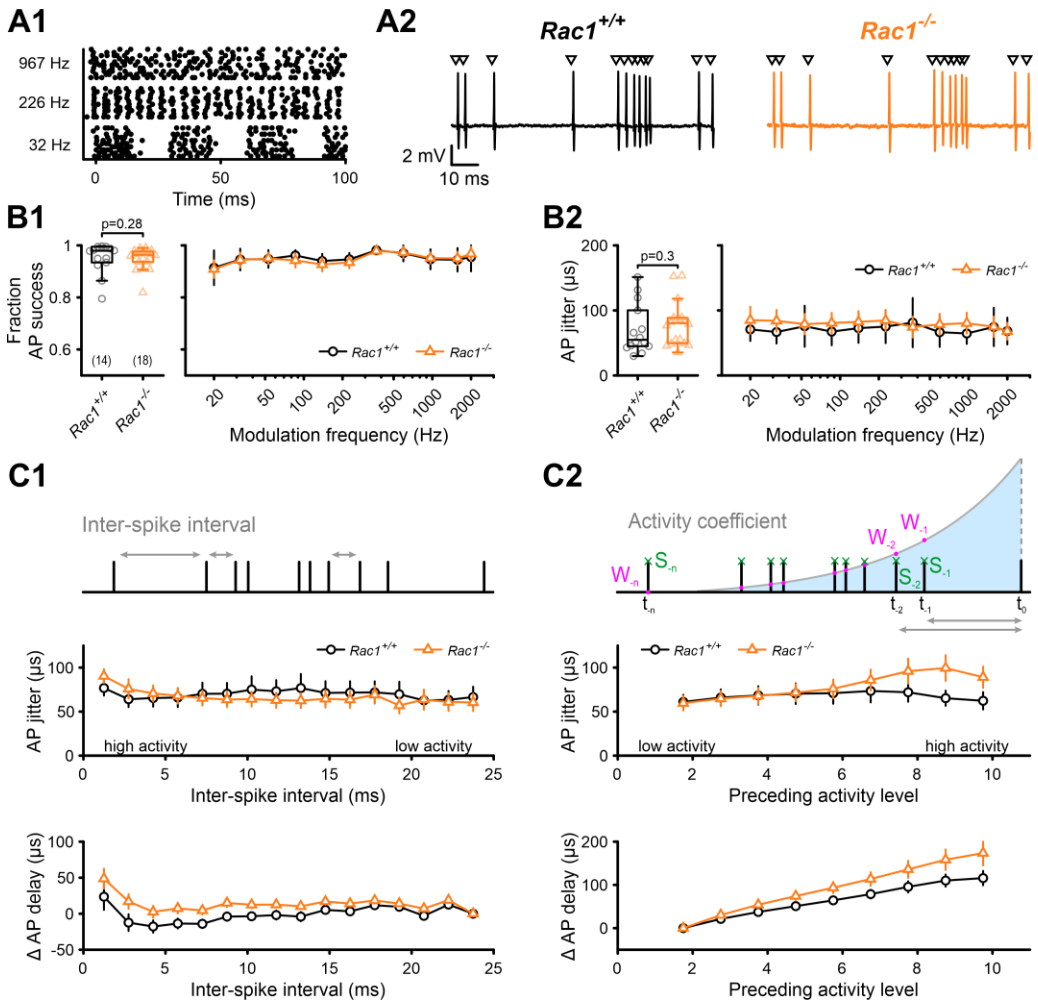

1023

1024 **Fig. 6: Alterations in presynaptic release probability did not impair the reliability of action**
1025 **potential generation during *in vivo*-like activity.** (**A1**) AP firing was recorded in response to *in*
1026 *vivo*-like stimulation patterns derived from responses to sinusoidal amplitude-modulated sounds
1027 at different modulation frequencies. Raster plot shows three representative stimulation patterns
1028 (**A2**) Representative traces of loose-patch recordings during afferent fiber stimulation with in vivo-
1029 like activity for *Rac1*$^{+/+}$ (black) and *Rac1*$^{-/-}$ (orange). (**B1**) Fraction of successful AP generation was
1030 not different between *Rac1*$^{+/+}$ and *Rac1*$^{-/-}$ independent of modulation frequency (**B2**) AP jitter
1031 defined as the standard deviation of AP latencies was not changed in *Rac1*$^{-/-}$ neither for the
1032 complete stimulus nor as a function of stimulus modulation frequency. (**C1**) AP jitter and AP delay
1033 as a function of preceding inter-spike interval (**C2**) AP jitter and AP delay as a function of preceding

1034 activity level. Note the increased AP jitter and AP delay in *Rac1*$^{-/-}$ at higher activity levels. The

1035 results of statistical tests are summarized in Table 1.

1036

1037

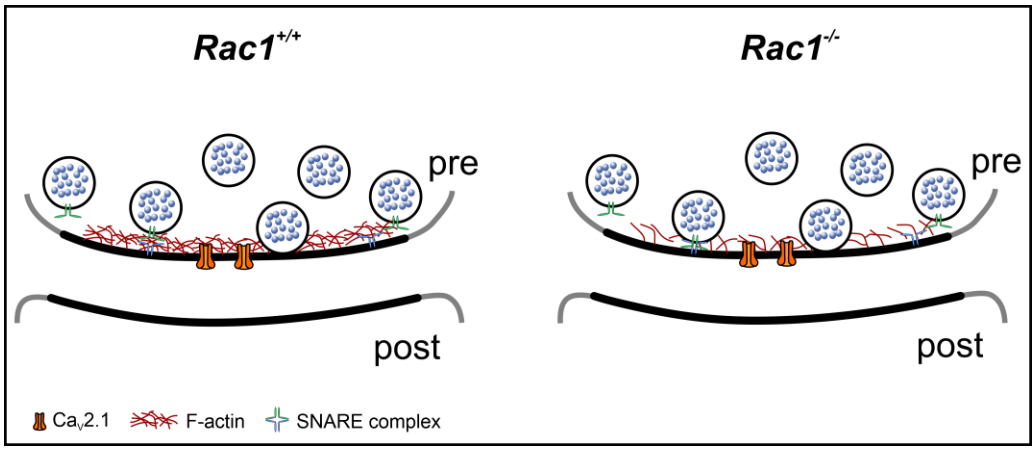

1038 **Fig. 7: Proposed model of Rac1's presynaptic role in regulating synaptic transmission.** In
1039 the proposed model loss of Rac1 results in changes in F-actin at the active zone, thereby reducing
1040 the barrier function between SVs and the plasma membrane. The resulting increase in SV
1041 fusogenicity increases Pr and synaptic strength.

1042